INL/RPT-24-80304-Revision-0

Comparison of Results between the Legacy and Refined RELAP5-3D Models of the High Temperature Test Facility in Exercises 1 and 2 of the HTTF Benchmark

Robby Kile, Jonathan Louis Barthle, Aaron S Epiney

Changing the World's Energy Future

Idaho National Laboratory

INL is a U.S. Department of Energy National Laboratory operated by Battelle Energy Alliance, LLC

DISCLAIMER

This information was prepared as an account of work sponsored by an agency of the U.S. Government. Neither the U.S. Government nor any agency thereof, nor any of their employees, makes any warranty, expressed or implied, or assumes any legal liability or responsibility for the accuracy, completeness, or usefulness, of any information, apparatus, product, or process disclosed, or represents that its use would not infringe privately owned rights. References herein to any specific commercial product, process, or service by trade name, trade mark, manufacturer, or otherwise, does not necessarily constitute or imply its endorsement, recommendation, or favoring by the U.S. Government or any agency thereof. The views and opinions of authors expressed herein do not necessarily state or reflect those of the U.S. Government or any agency thereof.

INL/RPT-24-80304-Revision-0

Comparison of Results between the Legacy and Refined RELAP5-3D Models of the High Temperature Test Facility in Exercises 1 and 2 of the HTTF Benchmark

Robby Kile, Jonathan Louis Barthle, Aaron S Epiney

September 2024

Idaho National Laboratory
Idaho Falls, Idaho 83415

http://www.inl.gov

Prepared for the
U.S. Department of Energy
Under DOE Idaho Operations Office
Contract DE-AC07-05ID14517

Comparison of Results between the Legacy and Refined RELAP5-3D Models of the High Temperature Test Facility in Exercises 1 and 2 of the HTTF Benchmark

INL/RPT-24-80304

Advanced Reactor Technologies

SEPTEMBER 2024

Robert F. Kile,
Jonathan L. Barthle, and
Aaron S. Epiney

Idaho National Laboratory

Idaho National Laboratory

Battelle Energy Alliance manages INL for the U.S. Department of Energy's Office of Nuclear Energy

DISCLAIMER

This information was prepared as an account of work sponsored by an agency of the U.S. Government. Neither the U.S. Government nor any agency thereof, nor any of their employees, makes any warranty, expressed or implied, or assumes any legal liability or responsibility for the accuracy, completeness, or usefulness, of any information, apparatus, product, or process disclosed, or represents that its use would not infringe privately owned rights. References herein to any specific commercial product, process, or service by trade name, trademark, manufacturer, or otherwise, does not necessarily constitute or imply its endorsement, recommendation, or favoring by the U.S. Government or any agency thereof. The views and opinions of authors expressed herein do not necessarily state or reflect those of the U.S. Government or any agency thereof.

INL/RPT-24-80304

Comparison of Results between the Legacy and Refined RELAP5-3D Models of the High Temperature Test Facility for Exercises 1 and 2 of the HTTF Benchmark

Robert F. Kile,
Jonathan L. Barthle, and
Aaron S. Epiney
Idaho National Laboratory

September 2024

Idaho National Laboratory
Advanced Reactor Technologies
Idaho Falls, Idaho 83415

http://www.art.inl.gov

Prepared for the
U.S. Department of Energy
Office of Nuclear Energy
Under DOE Idaho Operations Office
Contract DE-AC07-05ID14517

Page intentionally left blank

INL ART Program

Comparison of Results between the Legacy and Refined RELAP5-3D Models of the High Temperature Test Facility in Exercises 1 and 2 of the HTTF Benchmark

INL/RPT-24-80304

September 2024

Technical Reviewer: (Confirmation of mathematical accuracy, and correctness of data and appropriateness of assumptions.)

LISE CHARLOT (Affiliate) Digitally signed by LISE CHARLOT (Affiliate)
Date: 2024.08.27 11:51:16 -06'00'

Name: Lise Charlot
Technical Reviewer Title — Date

Approved by:

8/28/2024

Michael E. Davenport
ART Project Manager — Date

8/30/2023

Michelle T. Sharp
INL Quality Assurance — Date

Page intentionally left blank

SUMMARY

Work conducted in Fiscal Year 2023 identified that RELAP5-3D was capable of reproducing trends in High Temperature Test Facility data during experiment PG-27 but was incapable of reproducing measured values. The primary cause of this discrepancy between RELAP5-3D results and experimental data was hypothesized to be a distortion in power density that was introduced by the radial nodalization of the model. We further hypothesized that a model with a finer radial nodalization would provide better results when compared to the experiments PG-27 and PG-29. Work this fiscal year developed a new model that is better capable of capturing local heat generation rates and contains a representation of each 1/6 azimuthal sector of the core. We used this model to develop a new set of solutions to Exercises 1 and 2 of Problems 2 and 3 of the OECD/NEA HTGR T/H benchmark. In this report, we present the first comprehensive comparison of the results between the 2 models. We see that in Exercise 1A, which is common between Problems 2 and 3, the results are similar, though the results from the new model show greater detail than those from the legacy model. In Problem 2 Exercise 1B and Problem 3 Exercise 1B, we see that heat removal is slower in the new model than the legacy model. Problem 3 Exercise 1C shows temperatures that are lower in most places in the new model than the legacy model, but the area with active heat generation has higher block temperatures in the new model than the legacy model. Problem 3 Exercise 1D further shows that long-term heat removal is lower in the new model. Problem 2 Exercise 1C demonstrated that the new model observes higher temperatures in the core regions than the legacy model, justifying the need to preserve the power density in the High Temperature Test Facility. The validation ofRELAP5-3D using PG-27 and PG-29 also demonstrated the improved temperature agreement in the core regions, particularly with a calibrated model that implements an effective thermal conductivity for the core material. Overall, PG-27 models show reasonable to excellent agreement for steady-state temperatures and minimal to reasonable agreement for transients. PG-29 models showed minimal agreement with the data.

Page intentionally left blank

CONTENTS

FIGURES

TABLES

ACRONYMS

DCC	depressurized conduction cooldown
ETC	effective thermal conductivity
Ex1A	Exercise 1A
Ex1B	Exercise 1B
Ex1C	Exercise 1C
Ex1D	Exercise 1D
HTGR	high-temperature gas-cooled reactor
T/H	thermal hydraulics
HTTF	High Temperature Test Facility
HTTR	High Temperature Engineering Test Reactor
INL	Idaho National Laboratory
MHTGR	Modular High-Temperature Gas-Cooled Reactor
OECD/NEA	Organization for Economic Cooperation and Development, Nuclear Energy Agency
P2	Problem 2
P3	Problem 3
PCC	pressurized conduction cooldown
PSR	permanent side reflector
RCCS	reactor cavity cooling system
RELAP5-3D	Reactor Excursion and Leak Analysis Program, Version 5, 3D
SAM	Systems Analysis Module
TC	thermocouple

Page intentionally left blank

Comparison of Results between the Legacy and Refined RELAP5-3D Models of the High Temperature Test Facility in Exercises 1 and 2 of the HTTF Benchmark

1. INTRODUCTION AND MOTIVATION

RELAP5-3D (Reactor Excursion and Leak Analysis Program, Version 5, 3D) is a widely used systems thermal hydraulics code developed by Idaho National Laboratory (INL). RELAP5-3D has been used extensively in high-temperature gas-cooled reactor (HTGR) modeling [1–5], but the code has not been validated for these applications. The validation basis for prismatic HTGRs is somewhat limited compared to light-water reactors. Peach Bottom Unit 1 and Fort St. Vrain were both prismatic HTGRs, but data from those reactors is not easily accessible for validation purposes. The High Temperature Engineering Test Reactor (HTTR) in Japan is a 30 MW prismatic HTGR that provides some data for validation purposes [6], but HTTR contains no instruments measuring in-core temperatures, and HTTR predictions are fundamentally multiphysics predictions rather than pure thermal hydraulics predictions. The Modular High-Temperature Gas-Cooled Reactor (MHTGR) 350 benchmark was developed to provide a set of problems for the code-to-code comparison of neutronics, thermal hydraulics, and coupled multiphysics calculations for prismatic HTGRs to assess code performance [1], but ultimately this benchmark contains no data for validation purposes.

The High Temperature Test Facility (HTTF) was built at Oregon State University to provide data for HTGR code validation. HTTF includes over 500 instruments, including thermocouples at several axial and radial positions to allow for comparison between predicted and measured temperature distribution within the core [7]. The HTTF is a scaled version of the General Atomics MHTGR. It is scaled ¼ in length and is rated for a thermal power of 2.2 MW. HTTF operates at a reduced pressure compared to the MHTGR, but as the facility was primarily intended to be used for depressurization transients, this scaling of pressure was considered acceptable [7]. In the spring and summer of 2019, HTTF was used in a series of experiments that now form the basis of the Organization for Economic Cooperation and Development and Nuclear Energy Agency (OECD/NEA) HTGR thermal hydraulics (T/H) benchmark [8]. This benchmark provides problems for three sets of HTGR T/H physics: hot gas mixing in the lower plenum (Problem 1), depressurized conduction cooldown (DCC; Problem 2 [P2]), and pressurized conduction cooldown (PCC; Problem 3 [P3]). For a more detailed description of the benchmark problems and exercises, we refer to reader to Reference [8] or to the benchmark specifications.

Previous work has contributed to or run this benchmark, using a RELAP5-3D model developed at INL and released in 2018 [9–14]. Validation work with that model generally showed an ability to predict trends in the HTTF data but difficulties reproducing measured temperature data during transients [11–14]. In previous work, we identified an underprediction of transient temperature rise and hypothesized that this could be largely explained by modeling assumptions made when the RELAP5-3D model was developed, well before the experiments [14]. To test this hypothesis, we developed a new RELAP5-3D model of HTTF with a finer radial nodalization and separate azimuthal sectors to capture the asymmetry of Experiments PG-28 and PG-29.

In this report, we first present a summary of the new model. We then exercise the new model to solve P2 and P3 of the benchmark. For Exercise 1 (Ex1) of both problems, we compare results between the legacy [9] and new RELAP5-3D models. For Exercise 2 (Ex2) of both problems, we compare results of the new model to data and results of the legacy model.

1.1 HTTF Instrumentation

For a complete review of HTTF instrumentation, we direct readers to the HTTF instrumentation plan [15]. A significant shortcoming in the HTTF instrumentation is the lack of measurement of the primary helium flow rate. During steady-state periods, the coolant flow rate can be estimated based on the helium temperature rise from vessel inlet to outlet (cold duct to hot duct). During periods where temperatures are changing, however, this approach is not reliable. The primary figures of merit in the validation work are temperatures of the block and helium gas. These are measured through thermocouples (TCs) distributed throughout the facility. Within the core, TCs are located at the top of the odd-numbered core blocks. Blocks are numbered from the bottom up, with Block 1 being the block just above the lower reflector and Block 10 being the top block just below the upper reflector. The radial positions of the block TCs can be seen in Figure 1. The core of HTTF is divided into one-sixth azimuthal sectors, as seen in Figure 1. Of these six sectors, only three of them are instrumented. In order of a decreasing amount of instrumentation, they are referred to as the primary, secondary, and tertiary sectors. Only the primary sector has a TC at Position 1. Aside from the TC at Position 18, all TCs are R-type TCs, and their uncertainty is given by the relationship below [15]:

$$\sigma_{total}[°C] = \begin{cases} 3.285, 0° \; C < T < 600°C \\ \sqrt{2.174^2 + (0.004 \times T[°C])^2}, 600°C < T < 1450°C \end{cases}$$

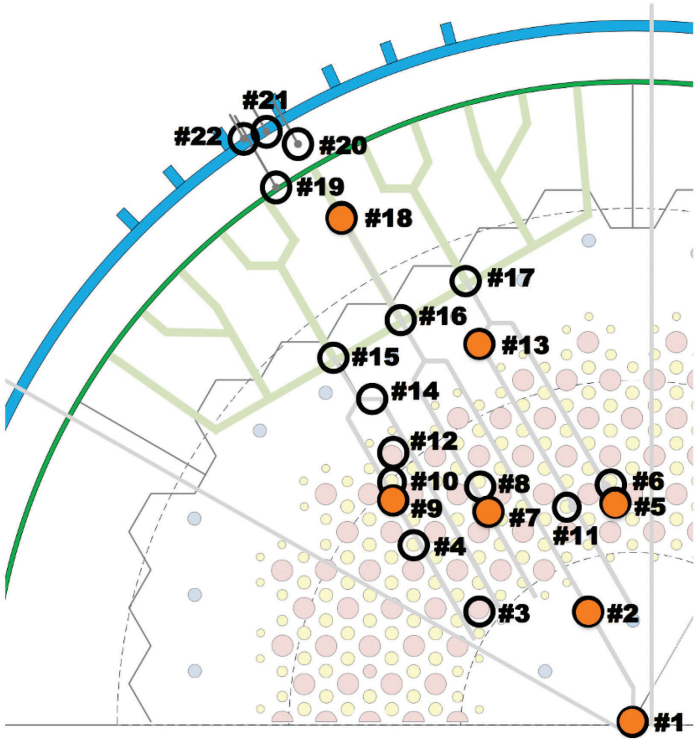

Figure 1. Block temperature TC radial positions used in previous analysis, highlighted in orange. Helium TCs are at Positions 6, 8, and 10. Reproduced from [14].

The TCs at Position 18 are K-type TCs, and their uncertainty is given by the relationship below [15]:

$$\sigma_{total}[°C] = \begin{cases} 2.142, 0° \; C < T < 275°C \\ \sqrt{1.838^2 + (0.004 \times T[°C])^2}, 275°C < T < 1250°C \end{cases}$$

1.2 Code Assessment Descriptors

In the early 1990s, the U.S. Nuclear Regulatory Commission worked to provide a way to categorize the performance of computer models against experimental data. This effort led to the following code assessment descriptors, which will be used to provide some brief assessment of the performance of the legacy model and will be used when assessing the validation of the new model. There are four levels of agreement [16]:

- **Excellent Agreement**: The model shows no deficiencies in predicting the results. Results from the model are within the uncertainty of the measured data. Using this model for this application will yield correct results.
- **Reasonable Agreement:** The model shows a few minor deficiencies in predicting results, but the major trends in the data are captured well. Predictions from the model may lie slightly outside the uncertainty bands of the data. Using this model for this application will yield accurate conclusions, though specific values may not be correct.
- **Minimal Agreement:** The model exhibits significant deficiencies in predicting results. Results from the model are well outside the uncertainty in the data. Predictions from the model are generally not acceptable but may be under some limited circumstances. Some major trends may be predicted correctly. Using this model for this application may lead to incorrect conclusions.
- **Insufficient Agreement:** The model has significant deficiencies and cannot provide an acceptable prediction of the results. Major trends are not well predicted, and model predictions are almost always well outside the uncertainty bands of the data. Use of the model for similar applications is likely to lead to incorrect conclusions.

These are referred to as "code assessment descriptors," but the word "model" is used instead of "code" in the descriptions provided above. We chose to use the word "model" instead of "code" to highlight the fact that a code validated for a given application can still provide incorrect results if the code is not used correctly. This is alluded to in the Nuclear Regulatory Commission reports defining code assessment descriptors. When agreement is "reasonable" or "minimal," the report encourages modelers to revisit the nodalization of their models to ensure they are sufficiently detailed for the application at hand [16].

1.3 The Legacy RELAP5-3D Model

The legacy RELAP5-3D model is the one described in Reference [9]. This model has been used in several studies of HTTF experiments [11–14,17]. In the work by Halsted and Gutowska, RELAP5-3D was used to provide boundary conditions for computational fluid dynamics models of the lower plenum [17]. In that work, RELAP5-3D temperature predictions were not compared to measured data, but lower plenum results will be strongly impacted by the quality of the boundary conditions RELAP5-3D can provide.

The legacy model divides the core and reflectors into a series of concentric rings, as shown in Figure 2. The region marked as "central reflector" in Figure 2 is referred to as the "inner reflector" in this work; the "side reflector" is referred to as the "outer reflector" in this work, and the "permanent reflector" is referred to as the "permanent side reflector (PSR)." The active core region is divided into inner, middle, and outer rings. The inner and outer reflectors are also each modeled as three rings. In the active core, each ring contains dozens of coolant channels. In the inner reflector, the middle of the three rings contains the six inner reflector coolant channels. The 36 outer reflector coolant channels are contained within the middle outer reflector ring. A small gap is modeled between the outer reflector and the PSR, with heat being transported across that gap through radiation heat transfer. For a detailed description of the legacy model, we direct the readers to Reference [9].

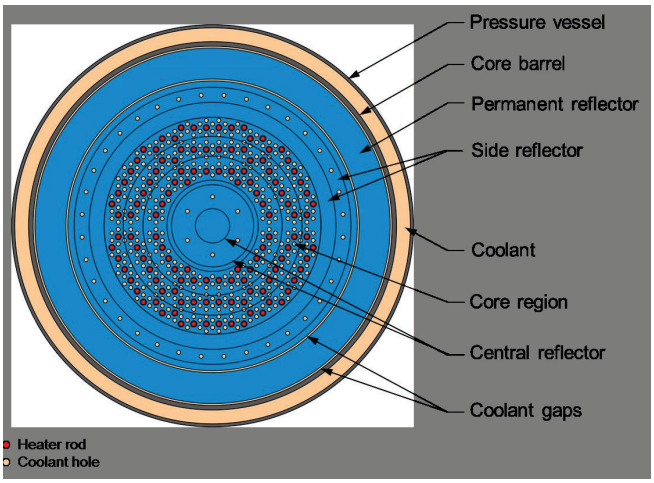

Figure 2. Radial nodalization diagram of the legacy RELAP5-3D model, reproduced from Reference [9].

Table 1 contains a summary of code assessment descriptors when the legacy RELAP5-3D model is applied to HTTF experiments. Heat generation in the PG-29 experiment is azimuthally asymmetric, and the legacy RELAP5-3D model is incapable of modeling that asymmetry, which is likely the main driver of the insufficient agreement between RELAP5-3D predictions and measured data for PG-29. Challenges with predicting PG-26 have largely been attributed to significant uncertainties in the state of the facility during the experiment due to a lack of steady state prior to the onset of the DCC and due to several confounding events that occurred during the experiment [11,12]. During the long steady-state portion of PG-27, the temperature distribution provides reasonable agreement with the data, but during the transient portion of the experiment, the agreement is minimal.

Table 1. Code assessment descriptors for the legacy model as applied to HTTF experiments.

Experiment	Code Assessment Descriptors	Reference
PG-26	Insufficient to Minimal Agreement	[11,12]
PG-27	Minimal to Reasonable Agreement	[13,14]
PG-29	Insufficient Agreement	[11,14]

We will not attempt to apply the code assessment descriptors to PG-28 modeling done by Halsted and Gutowksa [17], but they did note that “the inlet jet temperature distribution (obtained from R5 [RELAP5-3D]) is not consistent with what occurred in the experiment” [17]. They further noted that a channel-by-channel profile would be more appropriate for generating boundary conditions and suggested the legacy RELAP5-3D model could be altered to provide better agreement with experimental temperature results.

In general, an analysis of HTTF using the legacy RELAP5-3D model was found to predict trends in measured data but not reproduce measured values for considerable portions of the experiments modeled. Some of these discrepancies were attributed to the nodalization of the model; thus, we decided to build a new model with a finer radial nodalization and six azimuthal sectors capable of modeling asymmetry in the PG-29 experiment.

2. DEVELOPMENT OF THE NEW RELAP5-3D MODEL

To test the hypothesis that a model better capable of capturing local power distribution and of modeling azimuthal sectors would provide more insight into RELAP5-3D capabilities for HTGR T/H modeling, we developed a new model with a smaller unit cell to better resolve local effects. This new model is divided into six azimuthal sectors. Detailed development of the new model is presented in Reference [18]. In the new model, each ring captures heater rods at the same radial position, as opposed to the legacy model where each ring consists of heater rods at multiple radial positions. Figure 3 shows a view of the core, including the six sectors, and the geometry used to define the unit cell. Regions containing coolant channels are represented using a coolant-centered unit cell with volume fractions of the coolant and block calculated based on the local volumes of coolant and block. Each sector is connected to adjacent sectors through conduction enclosures, and at the center of the inner reflector is the central cylinder, which is connected to each sector. The inner reflector coolant channels are represented with a unit cell, as are the outer reflector coolant channels. The outer part of the outer reflector and the permanent reflector are each modeled as annuli with the heat structure surface area terms one-sixth of the surface area of the actual annulus surface area. This approach allows the radial conduction to occur with appropriate radial nodalization while still preserving the surface area of the one-sixth azimuthal sector. The helium gap between the PSR and core barrel is where the six sectors are merged back into a single 360 degree representation.

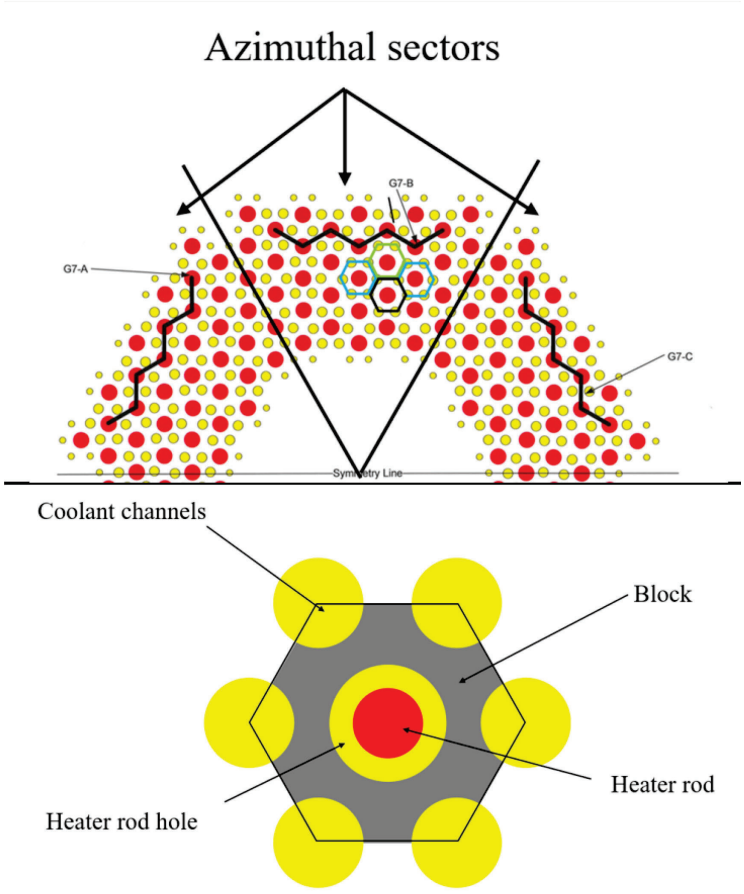

Figure 3. View of the core where each color of hex represents a “ring” (top) and unit cell view (bottom).

3. BENCHMARK RESULTS FROM NEW MODEL

Exercise 1 of both P2 and P3 is for code-to-code comparison between benchmark participants. Here, we present results from Ex1 for both the new and legacy models. P2Ex1 and P3Ex1 are broken into subexercises. The subexercises of P2Ex1 are:

1. Full-power steady state
2. DCC from full-power steady state
3. PG-29-like boundary conditions.

The extended steady state during PG-27 allows P3Ex1 to be broken down into four subexercises:

1. Full-power steady state
2. PCC from full-power steady state
3. PG-27-like low-power steady state
4. PG-27-like PCC.

P2Ex1A and P3Ex1A are identical in requested boundary conditions and outputs, so a discussion of both will be provided during the discussion of P2Ex1A. For P2Ex1C, implementing the transient boundary conditions was a significant task, and a comparison between the two models is not presented.

3.1 Problem 2

3.1.1 Problem 2 Exercise 1A

P2Ex1A represents a full-power steady state. The temperatures predicted in this exercise should be consistent with HTGR temperatures at full-power steady state. HTTF was never operated under these conditions, but this exercise provides an opportunity to compare code predictions when those predictions should be typical of HTGR temperatures. We compare coolant flow rate distributions, energy flows, and temperature distributions in this exercise. We expect the results from both models to be similar to one another, because this model has no azimuthal asymmetry and has a uniform power density distribution.

Table 2 shows the flow rate distributions in the new and legacy models. The terms “inner,” “middle,” and “outer” core are defined in the benchmark specifications and output templates for the benchmark. Dividing the core into these distinct regions provides the opportunity to compare mass flow rates on an “like-to-like” basis by comparing them over the same volume. The flow in the inner and outer reflectors of HTTF is considered bypass flow. The bypass flow fraction in the legacy model is 12.7% and 12.2% in the new model. These values are similar, but the value from the new model is more consistent with values predicted by other HTTF models [19]. We see in Figure 4 that helium temperatures are similar in the new and legacy models in most regions. In the inner reflector, coolant temperatures are lower in the new model than in the legacy model. We will discuss the reason for this result later. The helium temperature distribution from the new model shows lower temperatures at the very edges of the core region. This effect arises because the first and last rings in the core region do not contain any heater rods, so no power is being generated is those regions; only heat conducted from other rings to those rings is transferred to the coolant. We also see temperature peaks near, but not at, the edges of the core region. This arises due to the presence of both heater rods and small and medium coolant channels, leading to higher power-to-flow ratios in those regions. As we approach the middle of the core region, the coolant temperatures decrease and often approach the coolant temperatures in the legacy model. Coolant temperatures near the bottom of the core are generally slightly lower in the new model than the legacy model, and coolant temperatures near the top of the core are slightly higher than in the legacy model. Coolant temperatures in the outer reflector are higher in the new model than in the legacy model.

Table 2. Comparison of mass flow distribution between the new and legacy models.

	Inner Reflector	Inner Core	Middle Core	Outer Core	Outer Reflector
Number of Small Channels	—	24	0	72	—
Number of Medium Channels	—	30	0	66	—
Number of Large Channels	—	84	144	96	—
Legacy Model Flow Rate (kg/s)	0.0260	0.2311	0.3065	0.3351	0.1013
New Model Flow Rate (kg/s)	0.0261	0.2246	0.3120	0.3415	0.0958
Difference (kg/s, New—Legacy)	6.69e-5	-6.51e-3	5.54e-3	6.45e-3	-5.55e-3

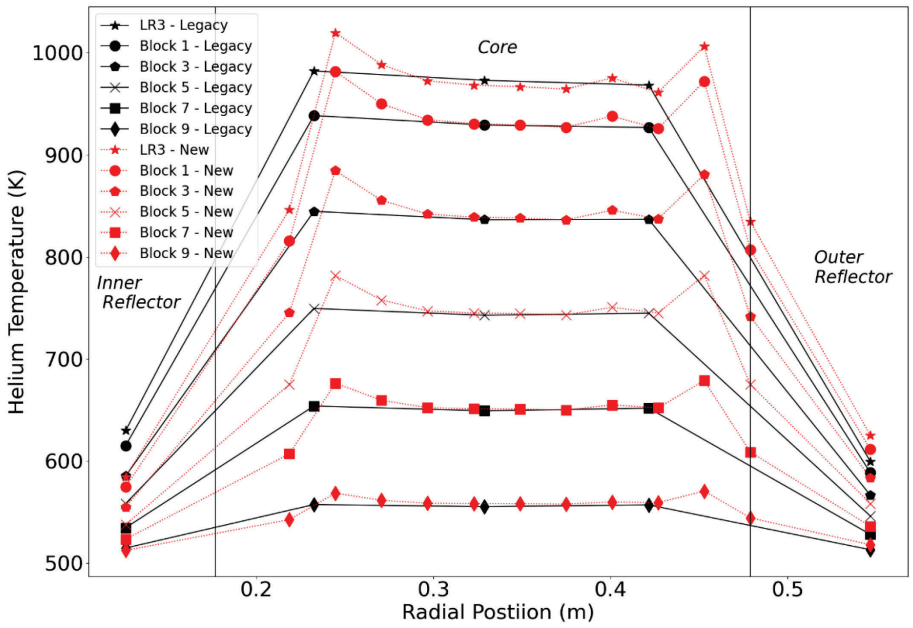

Figure 4. Helium temperature results from full-power steady state in both models.

Figure 5 shows block temperature distributions in the new and legacy models. We see similar trends in the block temperature comparison as we did in the helium temperature comparison, with the exception that the Block 9 temperature is lower in the new model than in the legacy model, whereas the helium temperature is just slightly higher in the new model than the legacy one. The temperature at the top of the lower reflector (LR3) is also lower in the new model than the legacy model. We note as well that temperatures in the first two parts of the outer reflector region are lower than in the legacy model. The last part of the outer reflector region corresponds to the PSR, and temperatures there show similar trends relative to the legacy model as helium temperatures in the core region do. The temperatures nearest the top and bottom of the core may be lower because the new model represents the entire axial length of a region using a single heat structure, whereas the legacy model used separate heat structures for the core length, upper reflector, and lower reflector. Using a single heat structure with axial conduction turned on leads to more realistic conduction than attempting to model axial conduction with conduction enclosures.

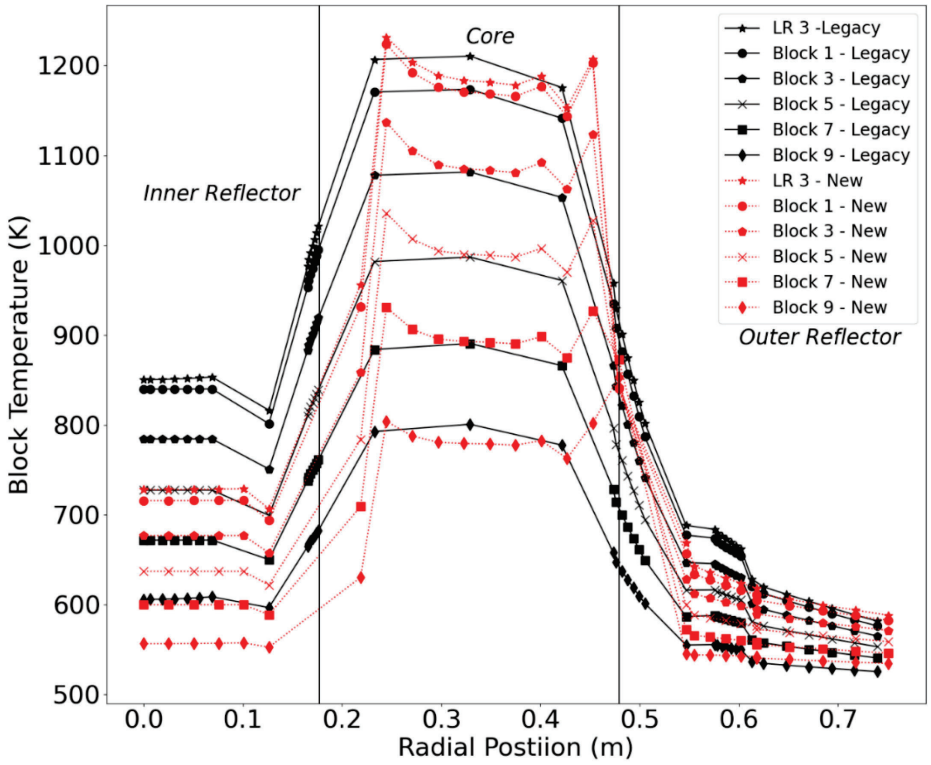

Figure 5. Block temperature results from full-power steady state in both models.

The block and coolant temperatures in the inner and outer reflectors are generally lower in the new model than in the legacy model. This is related to how the conduction enclosures and conductance tables are defined between the models. With the new model, each enclosure uses a unique temperature-dependent conductance table, whereas the same temperature-dependent conductance table was used in the legacy model, with variable conduction area factors to approximately scale the conductance from one enclosure to the next. Ultimately, this leads to a greater thermal resistance moving from the core region to the inner reflector, leading to lower temperatures in the inner reflector.

Table 3 shows a comparison of key energy balance values between the two models. We see that the new model has a slightly higher heat removal by convection in the core, the reactor cavity cooling system (RCCS) panels, and the RCCS cavity. The new model removes 2,186 kW through helium in the core, which is 1.6 kW higher than the legacy model. The RCCS panels remove 12.5 kW, 0.1 kW more than the legacy model. Rounding to the nearest tenth of a kilowatt, the new model removes the same amount of heat as the legacy model, but based on the slightly higher RCCS cavity air outlet temperature, we know that the new model removes slightly more energy than the legacy model through this channel as well. We note that the legacy model contained some radiation heat transfer pathways from the core to the upper and lower vessel heads, which do not exist in the new model. This would explain why the new model removes slightly more heat by convection.

Table 3. Energy balance results from P2Ex1A.

Region	Outlet Temperature Legacy/New (K)	Difference (K)	Power Removed, Legacy/New (kW)	Difference (kw)	Relative Difference in Power (% Legacy Model Value)
Reactor Vessel	921.2/921.7	0.5	2185.2/2186.7	1.5	0.07%
RCCS Panels	316.2/316.2	0.0	12.4/12.6	0.2	2%
RCCS Cavity	365.6/365.8	0.1	1.5/1.5	0.0	0%

Figure 6 compares core barrel and vessel temperatures between the new and legacy models. The core barrel temperature is slightly lower in the new model than the legacy one, but the vessel temperature is slightly higher. The new barrel temperatures are more consistent with those predicted by SAM and GAMMA+ [19], though the temperature being slightly lower at the bottom (LR 3) is different than is predicted by SAM (Systems Analysis Module) and GAMMA+. In both the new and legacy RELAP5-3D models, the vessel temperature has an initial decrease followed by a rise. The initial decrease in vessel temperature is an unexpected result but is consistent between models. This result should be consistent, because we did not change anything outside of the barrel in the new model. The temperature of the helium in the riser increases monotonically with increasing axial position, but the vessel temperature does not. Further investigation reveals that, along the length of the core barrel, the temperature drops when the length of the axial node changes. This is not a behavior that should arise, and it merits further investigation to determine if the relationship between change in node size and temperature drop is causal or if it is merely a correlation that arises from other factors.

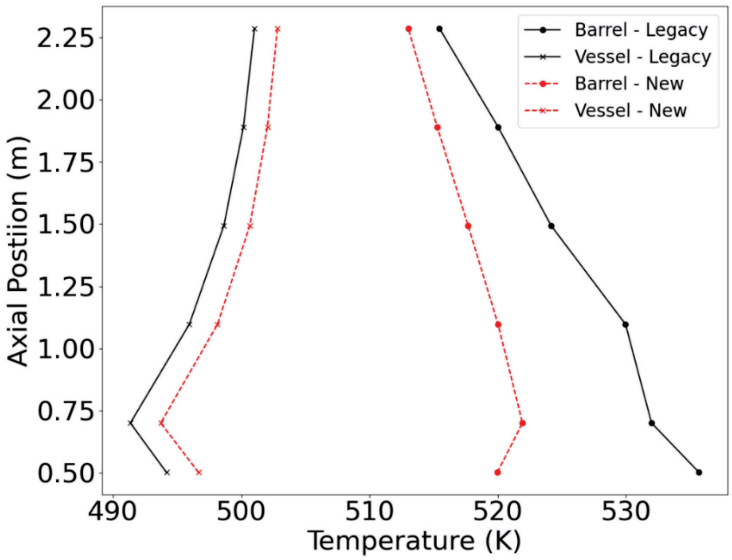

Figure 6. Core barrel and vessel temperatures in the new and legacy models.

In this section, we have presented the results for P2Ex1A from the new model, which will be the same as the results for P3Ex1A. Collection of P2Ex1A results was finalized on June 27, 2024.

3.1.2 Problem 2 Exercise 1B

This exercise represents a DCC occurring from a full-power steady state. This transient is initiated by decreasing the primary helium flow rate from 1.0 to 0.0 kg/s linearly over 1 second and depressurization linearly from 0.7 to 0.1 MPA over 20 seconds. At 0.0 seconds, the power is switched from the nominal 2.2 MW to the ANS-94 decay heat standard. Due to depressurization, natural circulation flow patterns are not established. Heat is transferred from the core to the reflectors through conduction, and as heat reaches the PSR, it is transferred to the core barrel, then the vessel, and then the RCCS through radiation heat transfer. Unlike Ex1A, helium outlet temperature is not a figure of merit in this exercise because of the lack of coolant flow. All figures of merit in this exercise are time dependent. The transient was run for 48 hours, at which point all temperatures had peaked, and all areas of the facility examined in this study were in cooldown. Results from the legacy model are also presented but are not a focus of discussion except as a point of comparison.

The temperatures in the inner portion of the inner reflector can be seen in Figure 7. In the new model, LR3 and Blocks 1, 3, and 5 all see a rapid temperature rise in the first 12 hours, followed by an extremely slow cooldown. Blocks 7 and 9 heat up much more slowly. The peak temperature in the inner reflector at Block 9 occurs at 40.15 hours and 39.625 hours for Block 7. The temperature reported here is the heat structure volume-averaged temperature of the inner cylinder heat structure for the legacy model, but for the new model, it is the temperature at the innermost node. The outer portion of the inner reflector is represented as a coolant-centered unit cell. Its temperatures are the heat structure volume-averaged temperature. Those temperatures are seen in Figure 8. Once again, we see that the locations near the bottom of the core see a rapid rise in temperature for the first 10–12 hours followed by a gradual cooldown. Block 7 sees its temperature increase for 18.15 hours, and the temperature in Block 9 rises for the first 38.05 hours. The helium temperature for the inner reflector shows similar behavior, as seen in Figure 9. All three figures for the inner reflector show significantly lower temperatures in the new model than the legacy model for much of the transient. Steady-state block temperatures in the inner reflector are also much lower in the new model than the legacy one. Both transient and steady-state results indicate that the thermal resistance between the core –where heat is generated – and the inner reflector is higher in the new model than the legacy model.

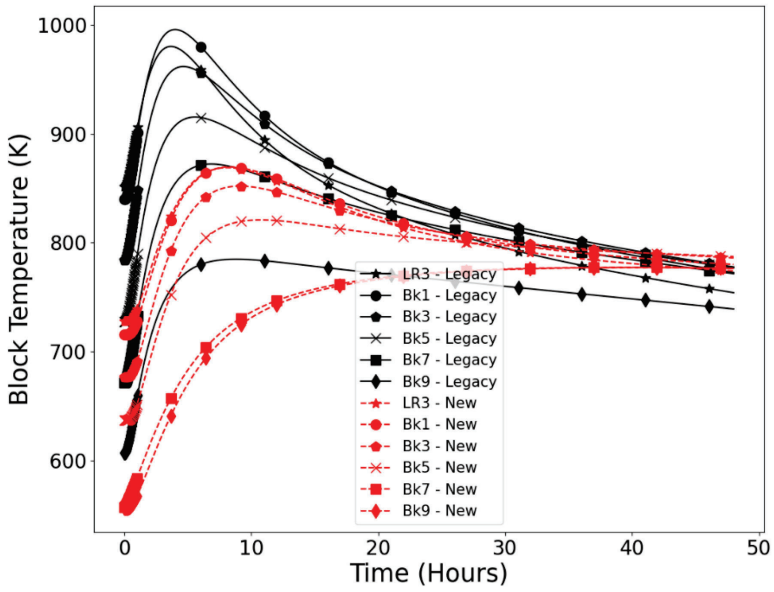

Figure 7. Block temperatures in the inner portion of the inner reflector during the DCC.

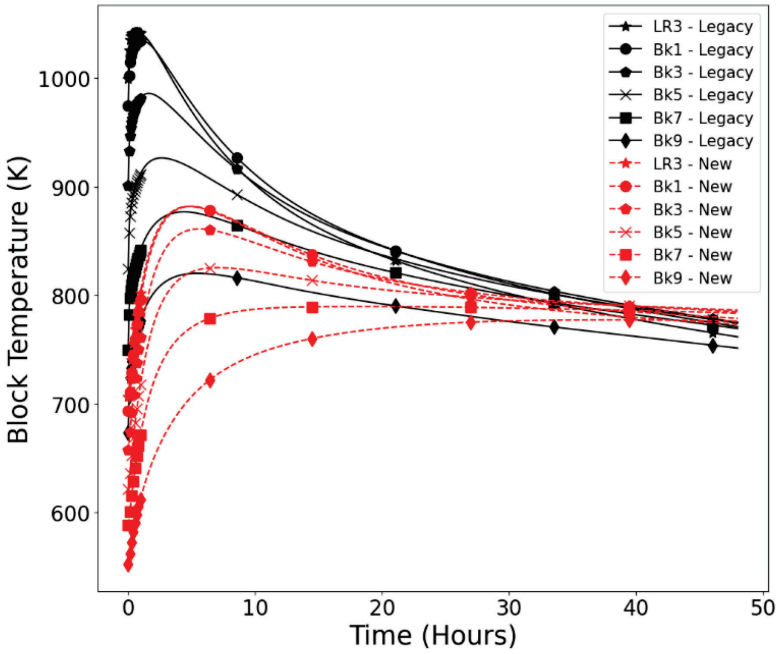

Figure 8. Block temperatures in the outer portion of the inner reflector during the DCC.

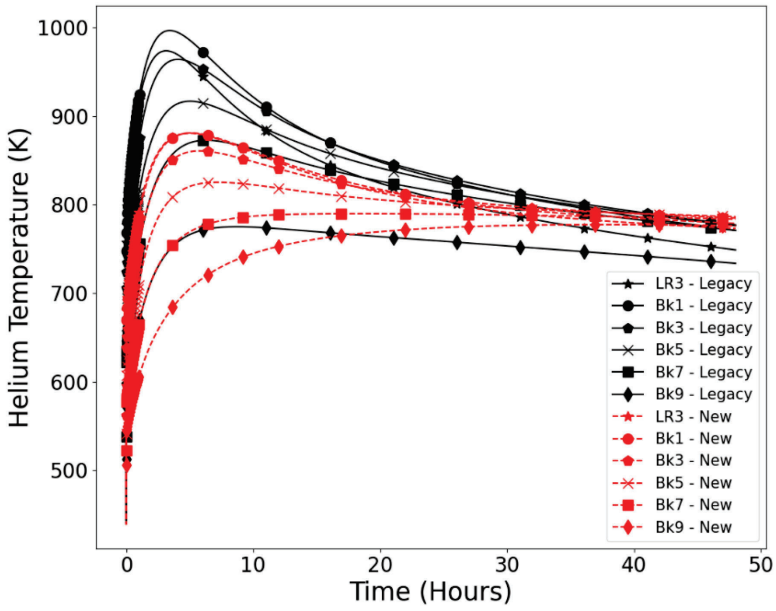

Figure 9. Helium temperatures in the inner reflector during the DCC.

Block temperatures in the inner core show a rapid increase following the cessation of forced flow; then, as heat gets redistributed inward, temperatures drop. Blocks 7 and 9 see a gradual reheating following the initial cooldown, and for Block 9, the temperature peaks at 34.4 hours, as opposed to within the first minutes of the accident. These results are seen in Figure 10, which compares the temperature of the inner ring in the legacy model to the equivalent space in the new model. The equivalent space was determined by volume-weighting the temperatures of the first five rings of the new model. The helium temperatures in the inner core were similarly mapped into a variable representing the volume-averaged helium temperature in the inner ring of the legacy model. The helium temperatures all reach their maximum during the initial peak rather than during the secondary heat-up period, as seen in Figure 11.

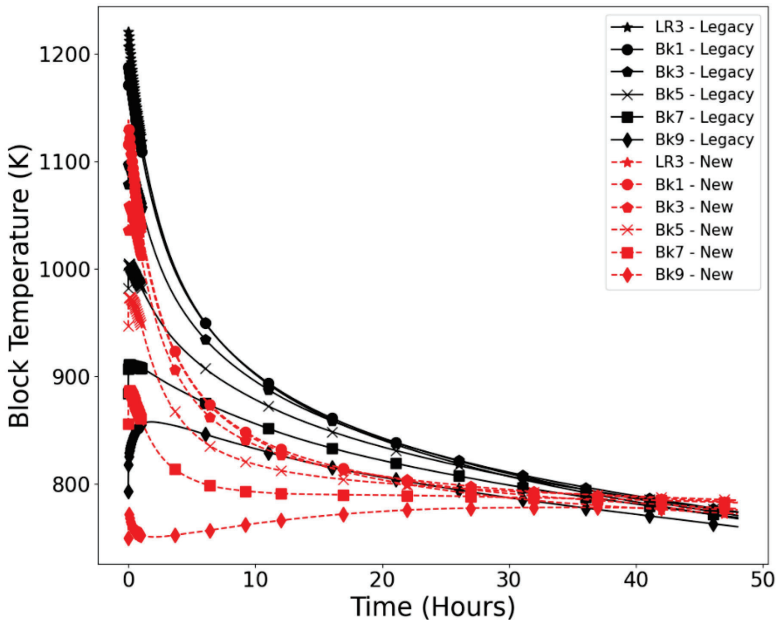

Figure 10. Inner core block temperatures during the DCC.

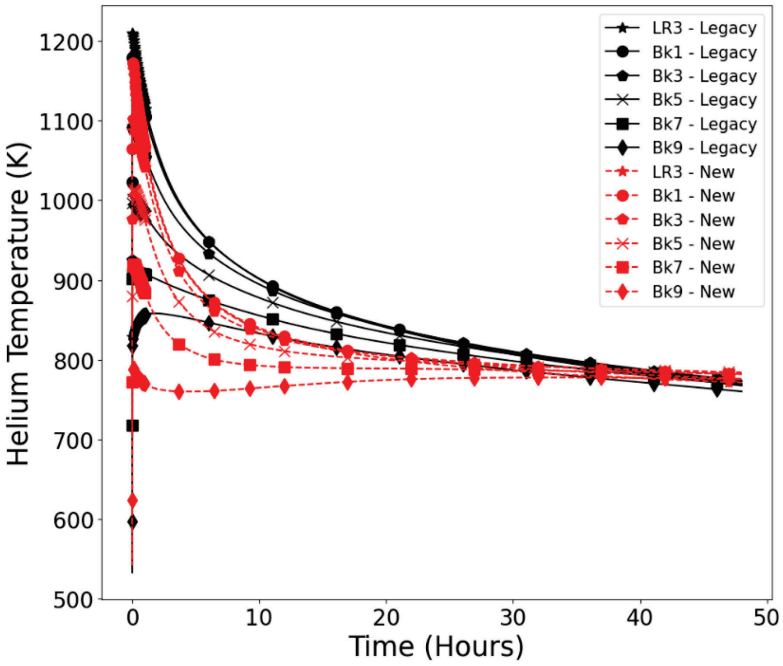

Figure 11. Helium temperatures in the inner core during the DCC.

In the middle core, the block temperatures all peak within the first few minutes of the accident, though the top does experience a secondary heat-up period (see Figure 12).The helium temperatures, as

shown in Figure 13, exhibit much the same behavior but with a more rapid initial rise. The temperature in Block 9 reaches its second, lower peak at approximately 39 hours.

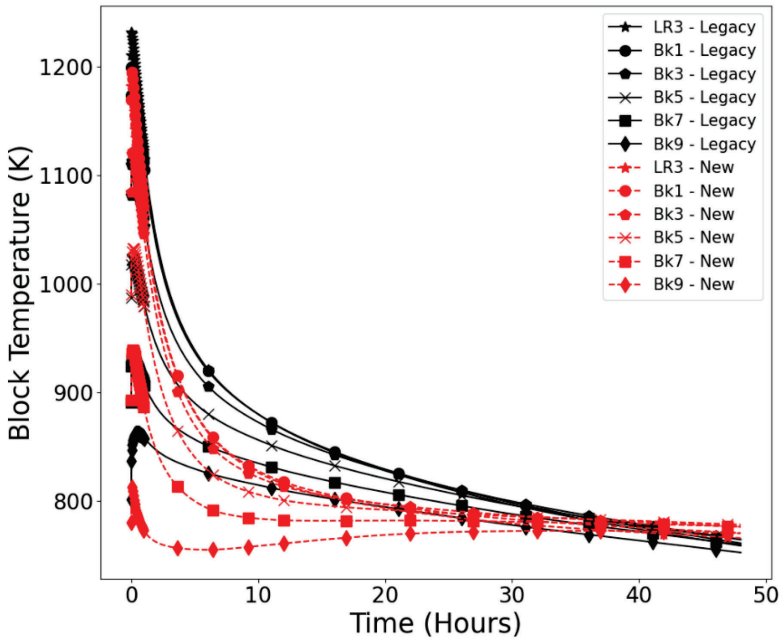

Figure 12. Middle core block temperatures during the DCC.

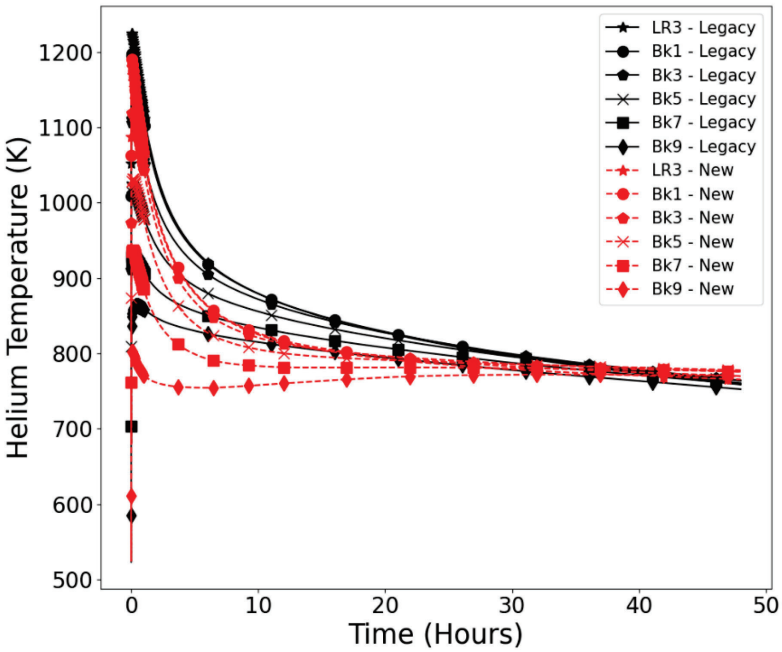

Figure 13. Middle core helium temperatures during the DCC.

Temperatures of both block and helium in the outer core exhibit similar behavior to the middle core, but with lower temperatures. Temperatures in the inner, middle, and outer core are compared over the same volumes between models, with the temperatures from the new model being mapped into the three ring space from the legacy model. This technique is not used for the inner and outer reflectors, so temperatures in the reflectors are not apples-to-apples comparisons, but they still provide some insight. As first shown in Figure 5, block temperatures in the outer reflector are initially lower in the new model than in the legacy model. Figure 14 shows that the outer reflector is slower to both heat up and cool down in the new model than in the legacy model. In the legacy model, the outer reflector inner piece is defined as the region between the outer core ring and the outer reflector coolant channels. In the new model, the outer reflector inner piece is defined as the entire region outside of the core but before the sawtooth region of the block, which can be seen in Figure 1. The region in the new model is larger than in the legacy model, and because it contains points that are farther from the core, the temperature should be lower than the one in the legacy model. More interesting than the magnitude of the temperature is the shape of the temperature vs. time graphs, which continue to indicate slower long-term heat removal in the new model than in the legacy one. The outer reflector inner piece is entirely in cooldown mode by 41.55 hours.

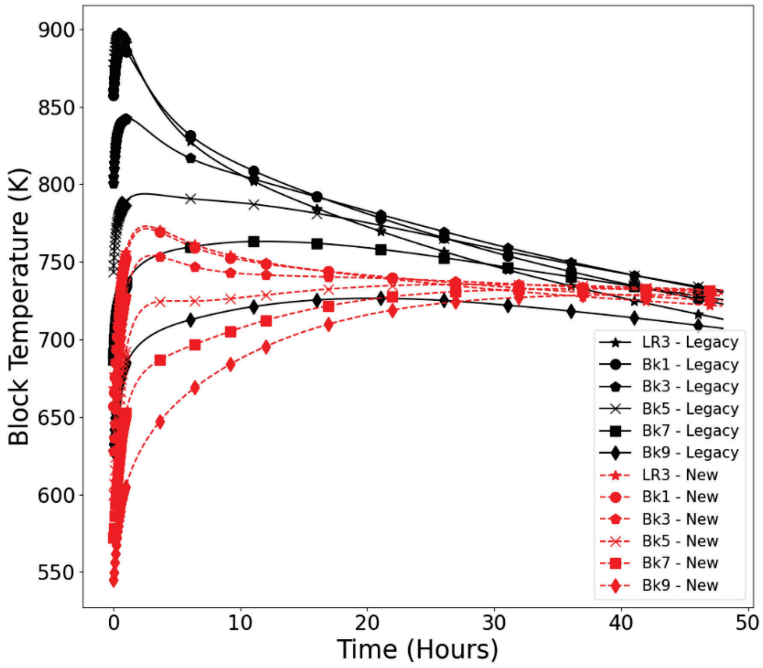

Figure 14. Outer reflector inner piece temperatures over time in the DCC.

Helium temperatures in the outer reflector exhibit somewhat different behavior than block temperatures. As shown in Figure 15, the helium in the outer reflector has a more rapid initial heat up in the new model than in the legacy model. Once again, however, it takes longer for the new model to reach the final long-term cooldown mode. The temperature of helium at Block 9 does not peak in the new model until 41.2 hours, as opposed to 27.5 hours in the legacy model. Block temperatures in the outer piece are, once again, not compared over the same volume, so some differences are expected. For example, the temperature in the new model is initially lower than in the legacy model, which is an expected result because the outer piece in the new model is smaller and starts farther from the core than in the legacy model. Again, block temperatures, as shown in Figure 16, show a slower heat up and a longer time until ultimate cooldown.

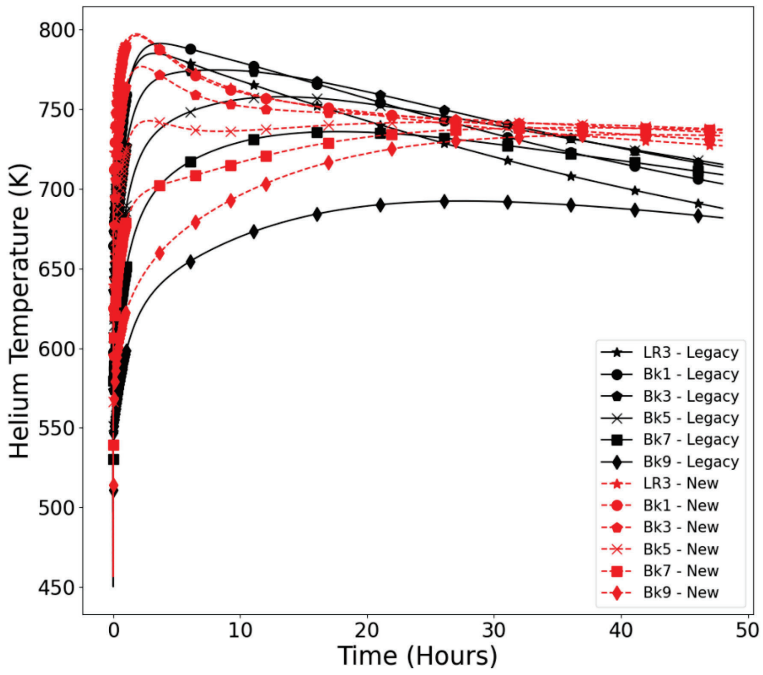

Figure 15. Outer reflector helium temperatures in the DCC.

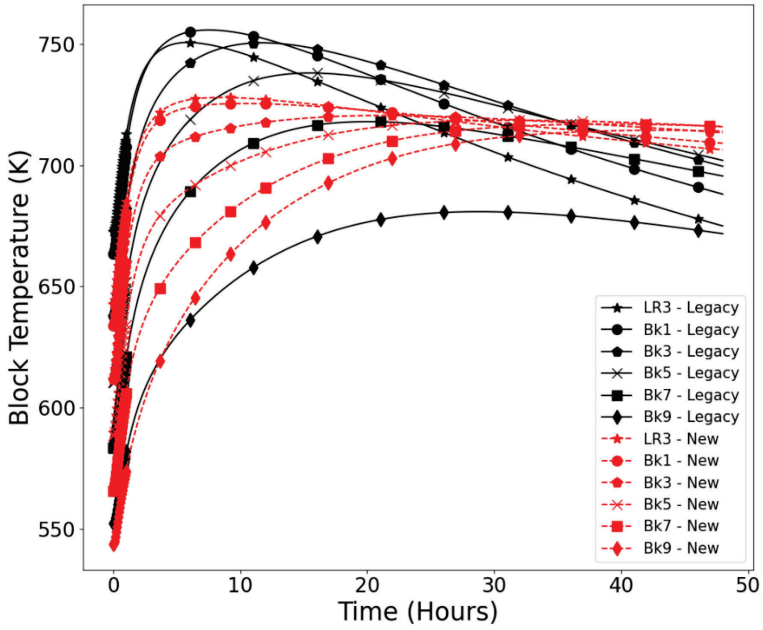

Figure 16. Outer reflector outer piece block temperatures.

Temperatures in the PSR are initially cooler at all locations except for Block 9. Again, results show a much slower heat up followed by a longer time until the model reaches cooldown. The peak Block 9 temperature in the new model is not reached until 45.55 hours, as shown in Figure 17.

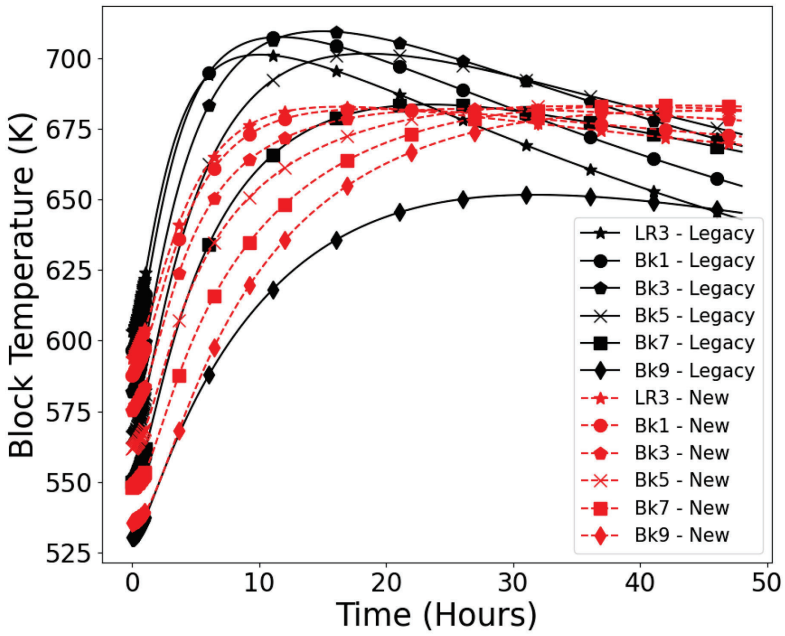

Figure 17. PSR temperatures over time in the DCC.

Comparison of the energy removed by the RCCS between the new and legacy models reveals that the RCCS removes heat more rapidly in the legacy model than in the new one. The initial drop in RCCS heat removal is much greater in the new model than the legacy one, and the heat removal rate never recovers. This can be seen in Figure 18. A similar trend is seen for RCCS water exit temperatures, though those are not plotted because they offer no additional insight. The radiation enclosures between the barrel and vessel and between the vessel and RCCS panels in the new model are the same as they are in the legacy model; therefore, the conclusion we can reach is that heat removal from the core and reflectors up to the barrel has been significantly slowed down in the new model. This is a result of the redesign of the conduction enclosures, perhaps driven by the switch from a radiation enclosure to a conduction enclosure between the outer reflector and the PSR. More detailed studies will be needed to determine exactly which changes led to this result.

We do not compare mass flow rates versus time in this section of the report, because the mass flow rate in the DCC is negligible. We will present a comparison of mass flow rates versus time in the P3Ex1B section.

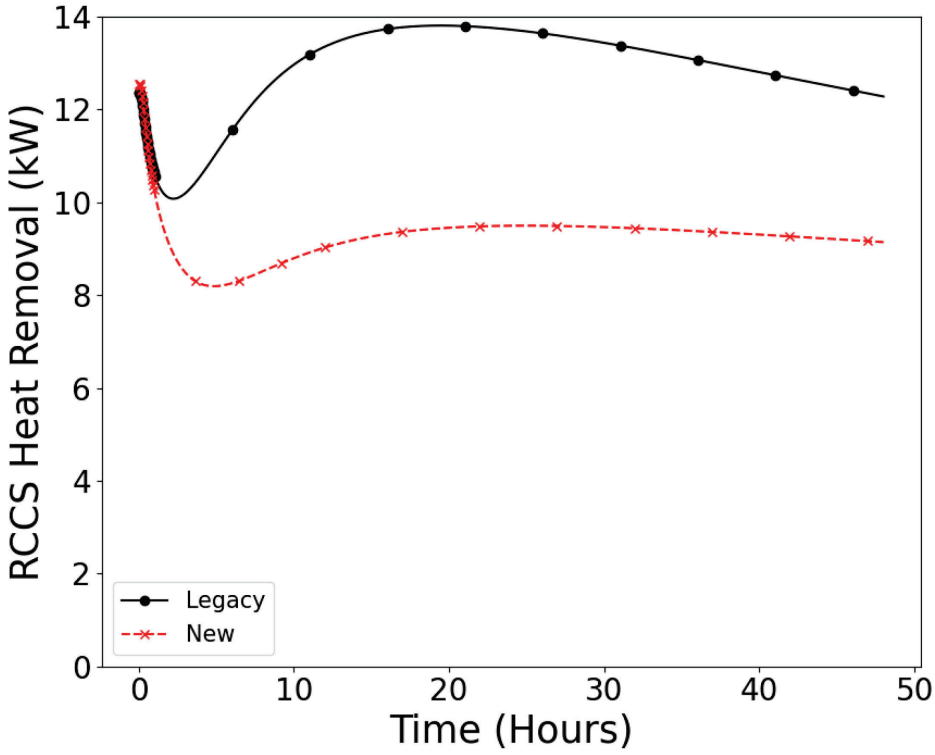

Figure 18. RCCS heat removal comparison in the DCC.

3.1.3 Problem 2 Exercise 1C

This exercise represents a simplified version of PG-29 in which the heat is distributed symmetrically in each sector. The power is distributed throughout the core, with some heat generation in each of the inner, middle, and outer core. The exercise starts with at low power, and after 8 hours, the DCC is initiated, power is ramped up then allowed to decay following a decay heat curve representative of the MHTGR. P2Ex1C focuses on implementing boundary conditions and initial conditions that are similar to that of the DCC, but around all 6 sectors to allow participants without sectorized models to take part in this exercise. These benchmark conditions were implemented into the new RELAP5-3D. Specifically, the heater configuration used for the primary sector of PG-29 was assumed for all sectors. The following section describes key results from the RELAP5-3D model utilizing the conditions outlined in P2Ex1C. Figure 19 depicts the temperature across the central cylinder of the inner reflector. We evaluated temperatures at multiple blocks to observe temperatures across the axial levels of the core. Before the onset of the transient, the temperature is highest towards the bottom of the core in Block 1. However, the peak temperature after the transient starts occurs towards the axial center of the core in Block 5, with a temperature of approximately 630 K.

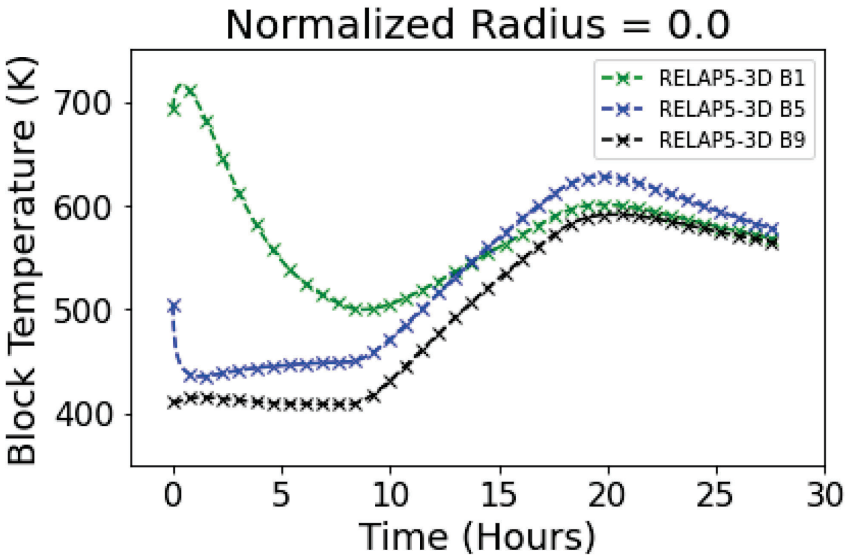

Figure 19. Temperatures within the central cylinder region.

The next set of temperatures were taken from the heated core region of the core. Specifically, these temperatures were taken at the third ring in the core. Figure 20 shows the temperature at Blocks 1, 5, and 9 for Ring 3 of the core block heat structure. Similarly, Figure 21 shows the coolant temperature for Ring 3 of the coolant channel at Blocks 1, 5, and 9. In both figures, the peak temperature for the core structure and primary coolant occurs in the midpoint of the core (Block 5) during the transient.

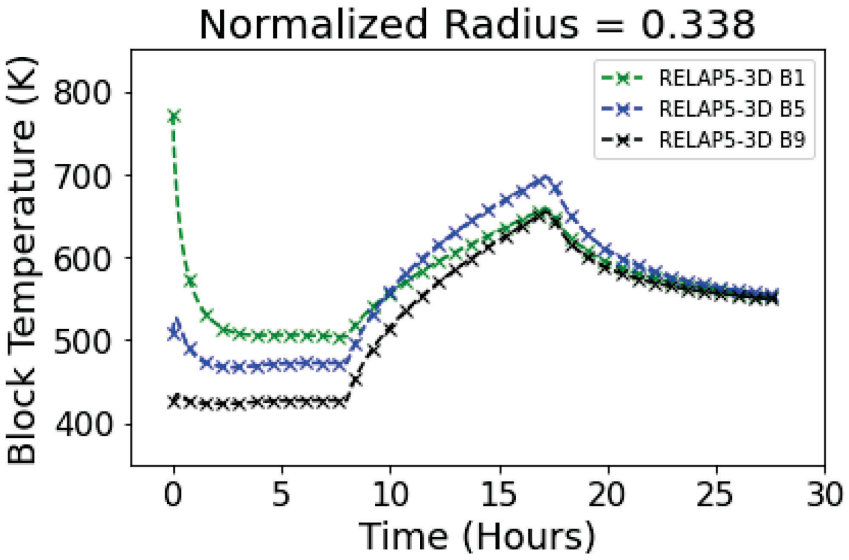

Figure 20. Temperatures within Ring 3 of the heated core.

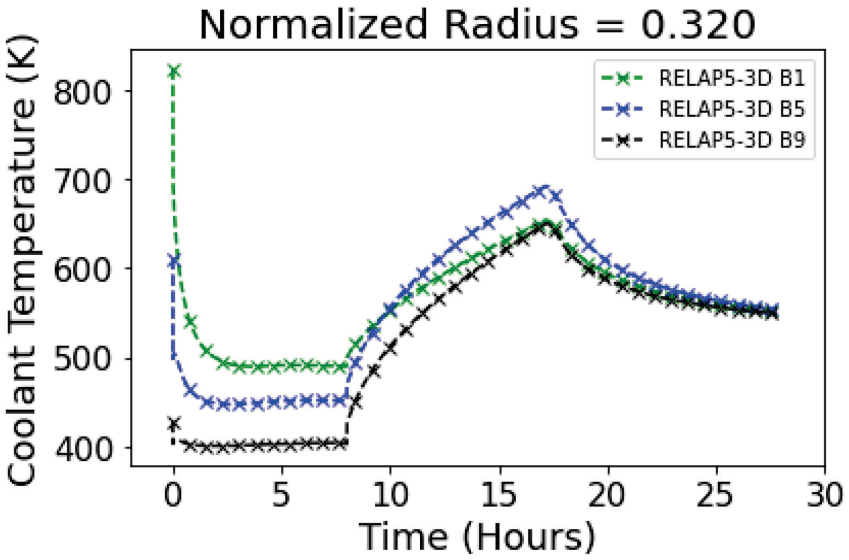

Figure 21. Temperatures throughout coolant channel in Ring 3 of the heated core.

In addition, Figure 22 and Figure 23 illustrate the temperatures in the outer shell and the PSR across Blocks 1, 5, and 9. As can be seen in both figures, there is not much axial variation in the temperatures in both the outer shell and PSR. The temperatures stay within about 50 K between the top and bottom of the reflectors.

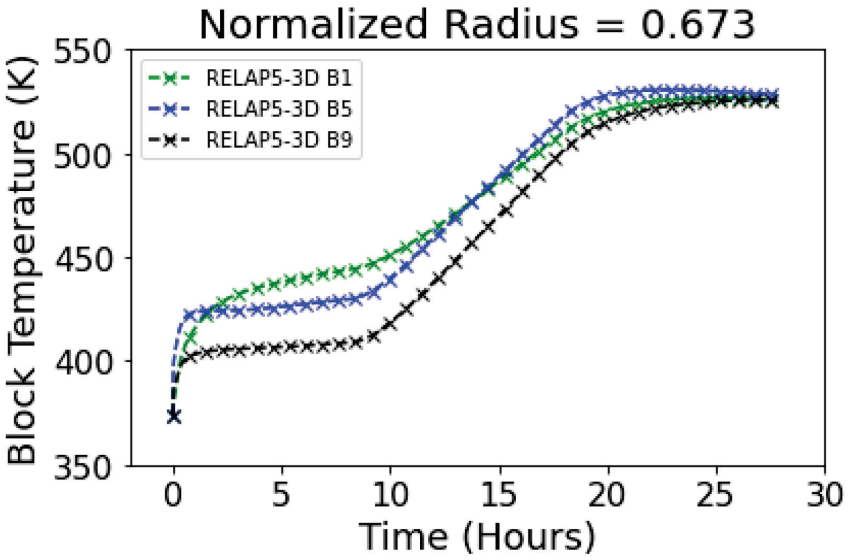

Figure 22. Temperatures across the outer shell.

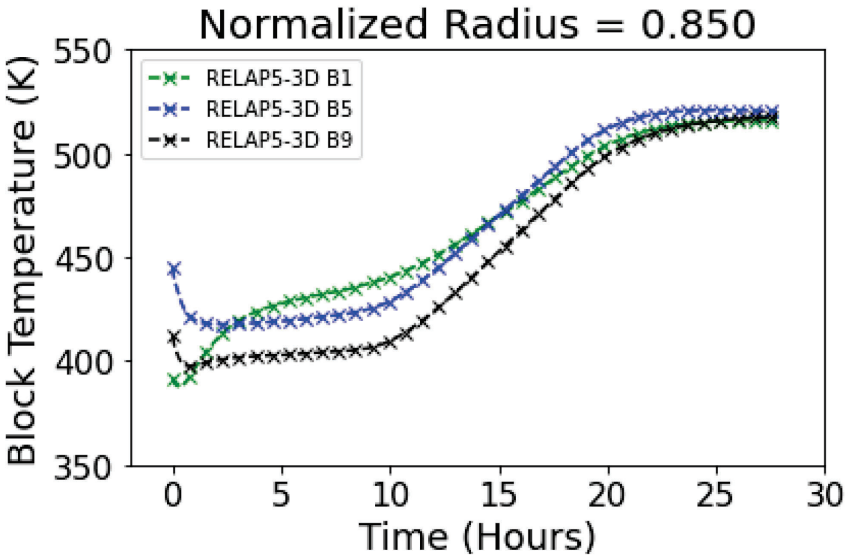

Figure 23. Temperatures across the PSR.

Finally, Figure 24 displays the RCCS coolant outlet temperature. The RCCS coolant outlet temperature starts at 290 K and quickly adjusts at the start of the transient to approximately 315 K. The outlet temperature then slowly increases over the course of the simulation.

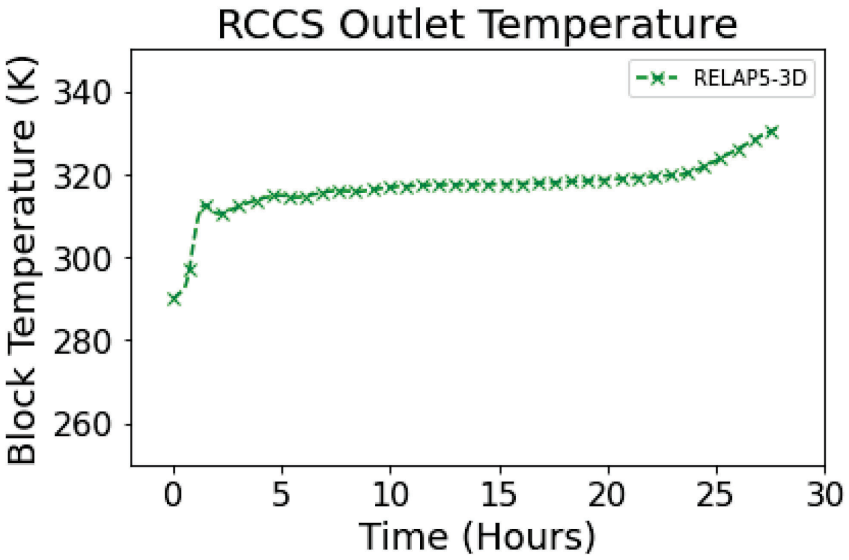

Figure 24. RCCS coolant outlet temperature.

A comparison of temperature predictions in the inner, middle, and outer core at block 5 between the new and legacy models can be seen in Figure 25. We see that the temperature drop following the initialization of the model is smaller in the new than in the legacy model. We also see that, following the onset of the DCC, the temperature rise is faster and the temperature drop following the deactivation of heater rods at approximately 15 hours is faster in the new model. This is consistent with the behavior we see in the core region in P2Ex1B, where the block temperatures in the core change more quickly in the new model.

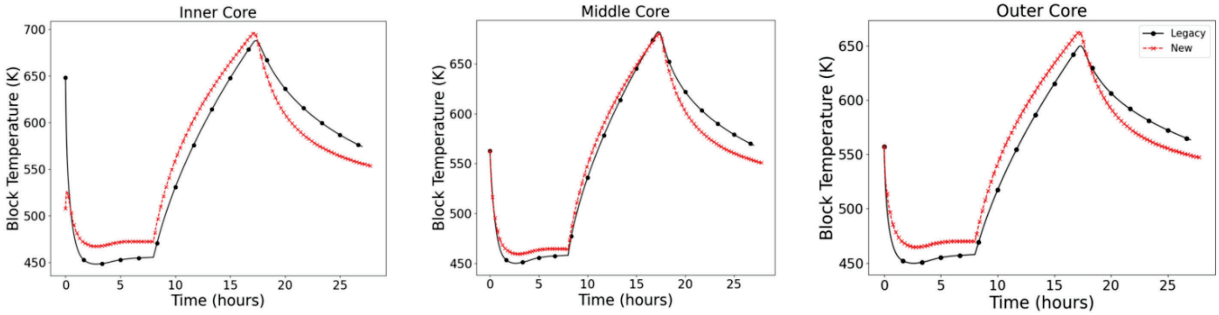

Figure 25. Block temperature distribution comparison between models at block 5

The temperature of the inner reflector central cylinder in both models during this exercise can be seen in Figure 26. The starting temperature is higher in the new model than the legacy one, but it converges towards the same temperature as the legacy model prior to the onset of the DCC at 8 hours. This is the only instance in which the new and legacy models show comparable temperatures in the inner reflector. Following the DCC, the new model heats up more slowly due to the greater thermal resistance between the heat source and the inner reflector. This is consistent with the trends from P2Ex1B.

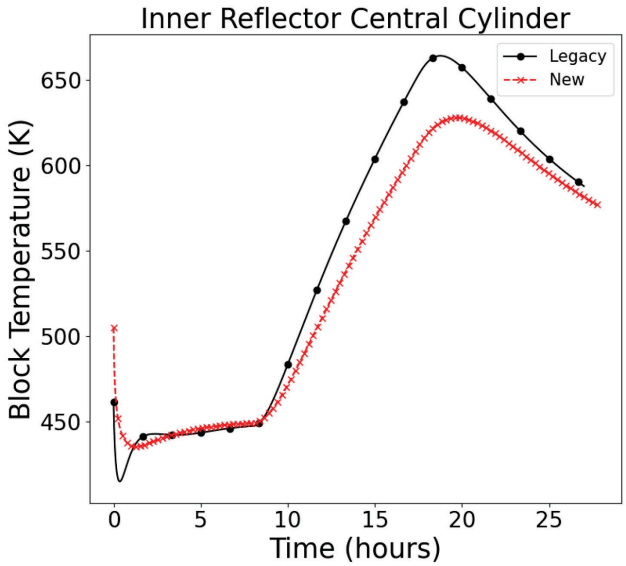

Figure 26. Inner reflector central cylinder temperature at block 5

Implementation of initial and boundary conditions for this exercise were more challenging than for Exercises 1A and 1B. This section primarily serves to demonstrate some benchmark results. The code-to-code comparison shows some consistent behavior with Exercise 1B. Core temperatures change more rapidly, but the inner reflector takes longer to respond and reaches a lower maximum temperature in this exercise. This further illustrates the significant differences in radial conduction between the new and legacy models.

3.2 Problem 3

3.2.1 Problem 3 Exercise 1A

Results from P3Ex1A are identical to those from P2Ex1A. Collection of P3Ex1A results was finalized on June 27, 2024.

3.2.2 Problem 3 Exercise 1B

This exercise represents a PCC from full-power steady state. At 0.0 seconds, the power transitions from steady to the ANS-94 decay heat standard. Starting at 0.0 seconds, the flow of helium is linearly ramped from 1.0 to 0.0 kg/s while the RCCS conditions remain unchanged from Exercise 1A. Following the cessation of forced flow, natural circulation patterns develop within the core which serve to redistribute heat within the core. Comparing results from P2Ex1B and P3Ex1B is not within the scope of the benchmark, but we do occasionally present some comparisons to P2Ex1B to demonstrate the impact of the natural circulation that arises in the PCC. The primary focus of this section, however, is the discussion of results from P3Ex1B, including a comparison between the new and legacy models. The model was run to a time of 48 hours, by which time temperatures everywhere in the core were dropping.

Temperatures in the inner piece of the inner reflector can be seen in Figure 27. Much like in Figure 7, the temperature at Block 9 rises slowly over many hours and visually may not appear to be dropping, but it is. The peak temperature of the inner reflector middle piece at Block 9 during the PCC is 763 K and occurs at 24.75 hours. In the DCC, the peak temperature in the same location is 777 K and occurs at 40.15 hours. This comparison is presented to show that the DCC is a more severe accident than the PCC.

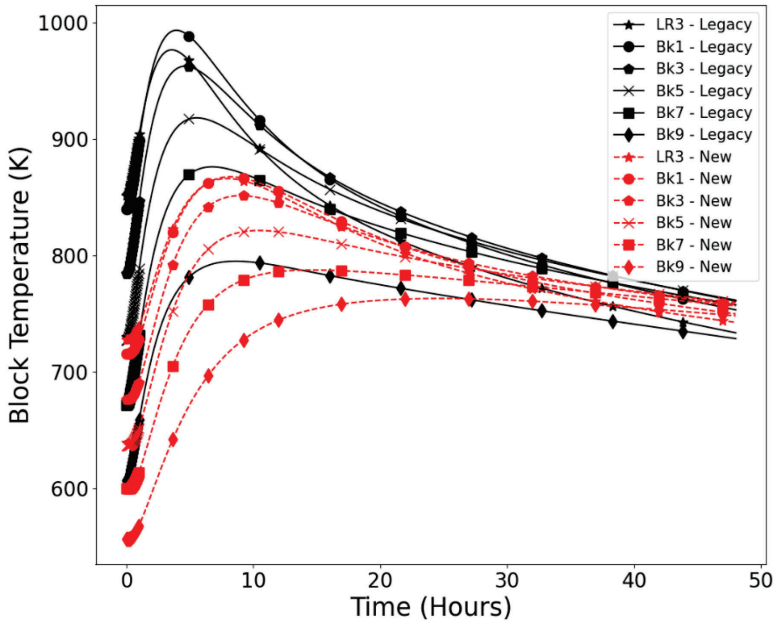

Figure 27. Temperatures in the inner piece of the inner reflector during the PCC.

The temperature in the outer piece of the inner reflector shows a similar trend to the inner piece. Figure 28 shows that, much like the inner piece of the inner reflector, temperatures start lower in the new model due to the increased thermal resistance between the core and inner reflector, and the heat up at the top of the core is slower in the new model, as is the long-term cooldown. For the outer piece of the inner reflector, the peak Block 9 temperature is 763.8 K and occurs at 22.45 K. This is slightly higher than the peak Block 9 temperature in the inner piece, but that is to be expected. This peak also occurs 2.3 hours earlier, but again, that is expected. Unlike block temperatures, helium temperatures (Figure 29) in the inner reflector start at similar values in both models. The new model, however, shows a smaller and slower rise in temperature, but the cooldown is also significantly slower.

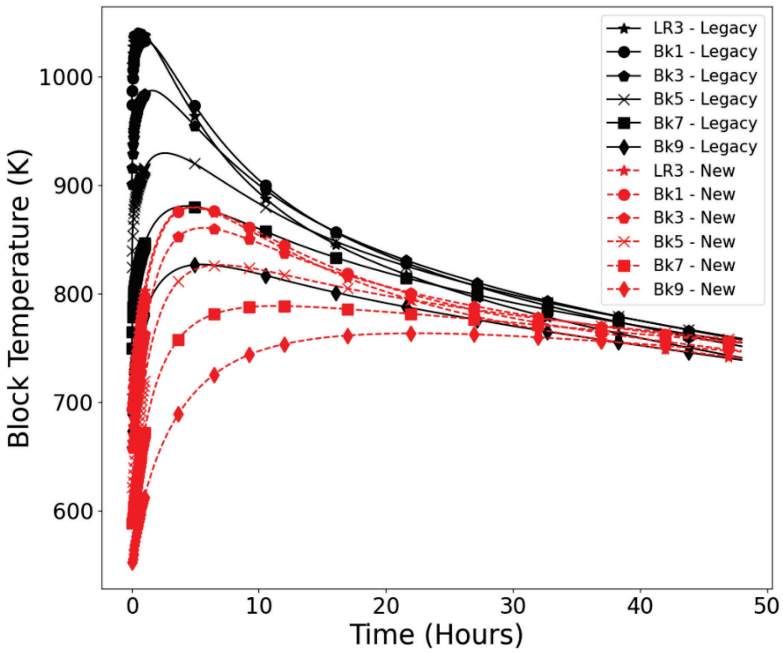

Figure 28. Block temperature in the outer piece of the inner reflector during the PCC.

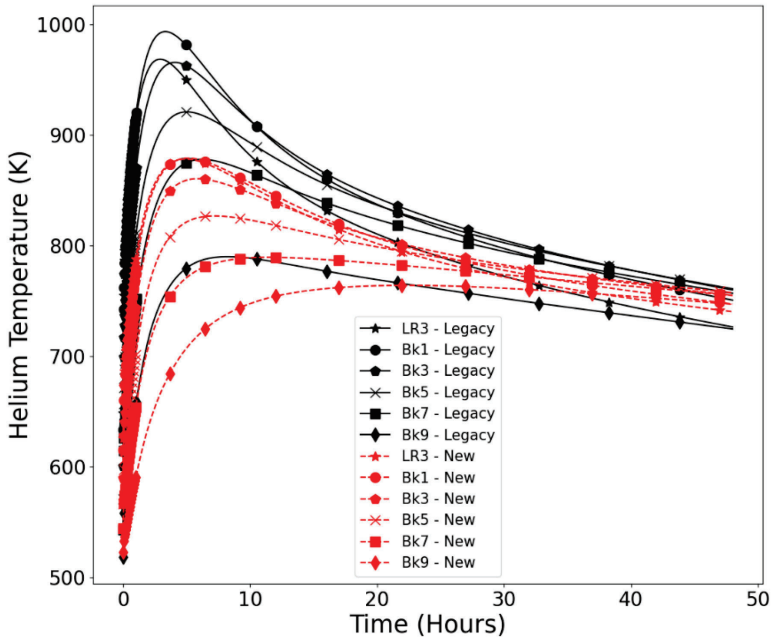

Figure 29. Inner reflector helium temperatures during the PCC.

Temperatures in the inner reflector generally show slower heat up and slower cool down in the new model than the legacy model. Temperatures in the core region, however, generally show a far more rapid initial cooldown in the new model than the legacy one. This can be seen in Figure 30 and Figure 31, which are representative of block and helium temperatures, respectively, in all three core regions. The new model shows a more rapid cooldown during the first 10 hours than the legacy model does, but the new model also shows a secondary heat-up period at Block 9. This arises due to axial conduction and heat redistribution from natural circulation.

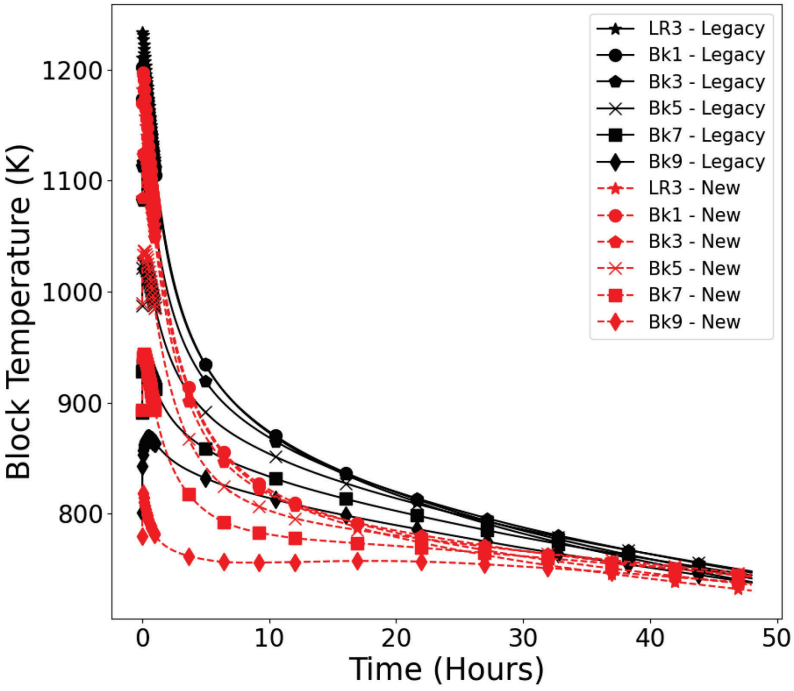

Figure 30. Block temperatures in the middle core region during the PCC.

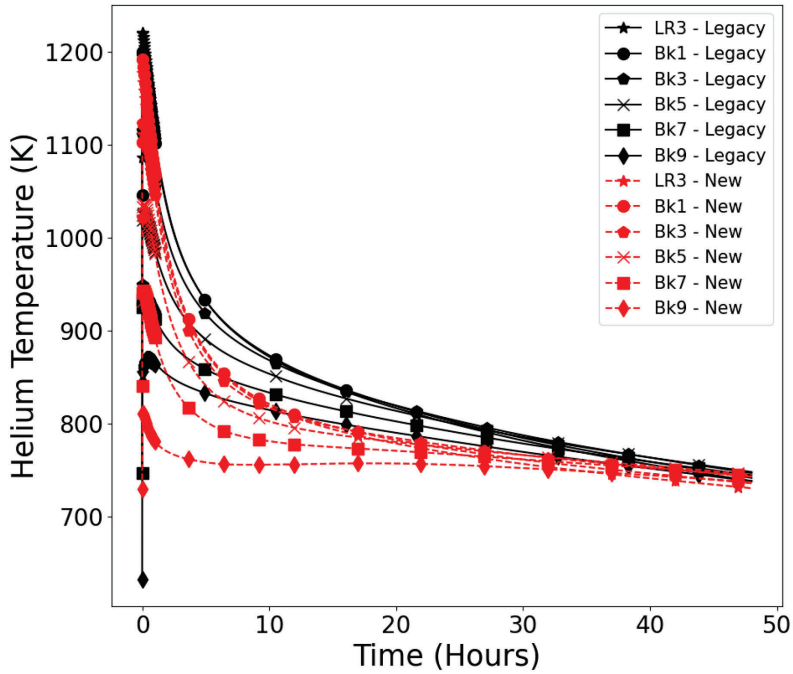

Figure 31. Helium temperatures in the middle core region during the PCC.

Helium temperatures in the outer reflector are shown in Figure 32. In the new model, the helium temperature in the outer reflector rises considerably faster than in the legacy model, but the cooldown is still lower. In the legacy model, the helium temperature in the outer reflector at Block 5 increases for the first 12 hours then decreases. In the new model, the outer reflector helium temperature at Block 5 peaks at 2.8 hours, then decreases at an initially decreasing rate for the next 10 hours, until the entire outer reflector enters cooldown. The block temperatures in the outer part of the outer reflector can be seen in Figure 33. Temperatures in the new model rise faster than in the legacy model, but peak temperatures at the bottom of the core are lower in the new model, and once again the long-term cooldown is slower.

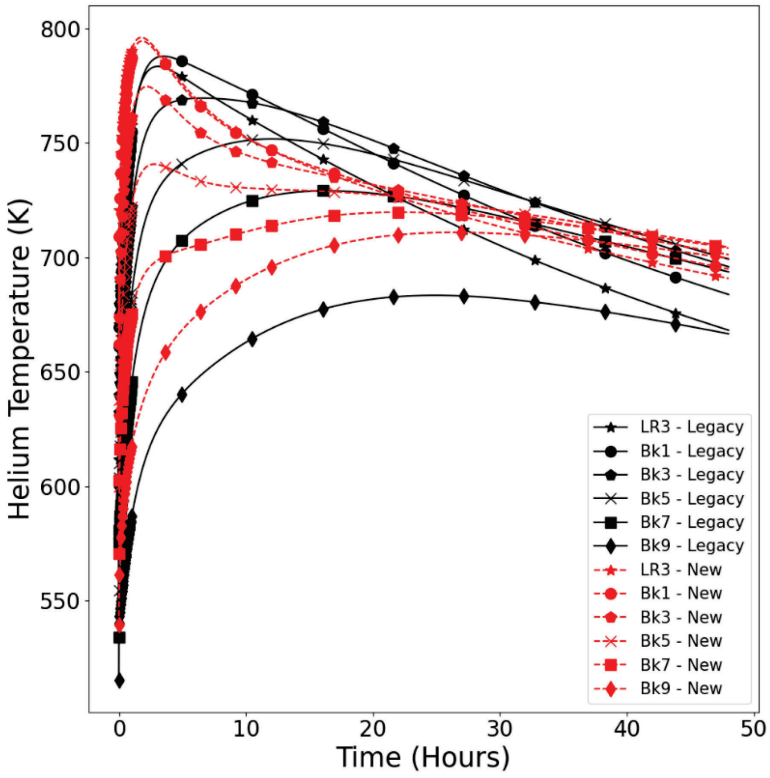

Figure 32. Outer reflector helium temperatures during the PCC.

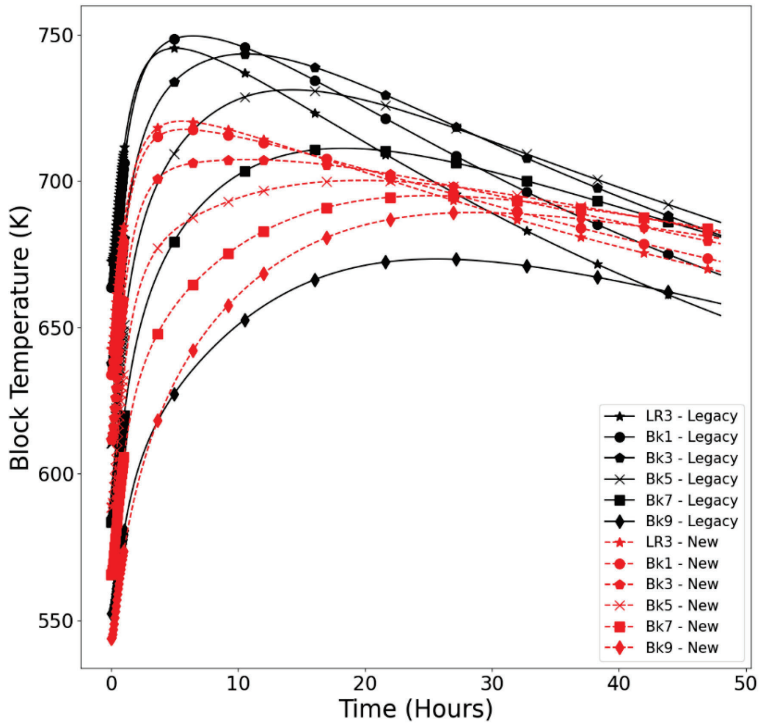

Figure 33. Block temperature in the outer portion of the outer reflector during the PCC.

The PSR temperature can be seen in Figure 34. The peak temperature at Block 9 in the new model is 653 K and occurs at 31.4 hours. Similar behavior is seen in the PSR as is seen in the outer reflector with regards to slower long-term cooldown. The temperature rise at upper blocks in the core is lower in the new model than in the legacy model, but at Block 9, the temperature rise is higher in the new model than the legacy model.

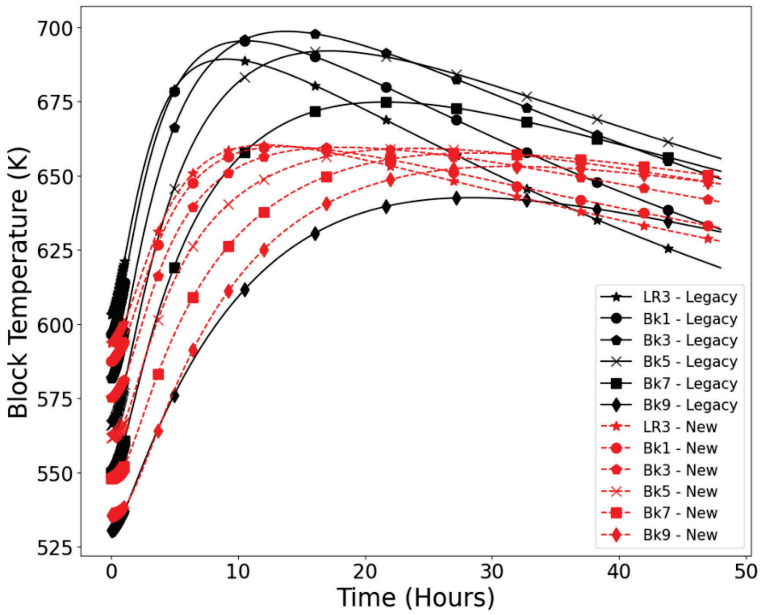

Figure 34. PSR temperatures during the PCC.

The slower long-term cooldown in the new model can be further seen in the RCCS energy removal rates, as shown in Figure 35. In both the PCC and the DCC, the new model removes heat less effectively than the legacy model; however, both models show greater heat removal during the PCC than the DCC. For both the PCC and the DCC, the new model shows that the peak energy removed by the RCCS occurs at t=0.0 seconds, but the legacy model shows peak RCCS heat removal rates greater than the steady-state heat removal. All four sets of results (two models and two transients) show an initial dip in RCCS heat removal. Table 4 shows that the minimum heat removal is lower for the new model in both transients and the minimum heat removal occurs during the DCC for both models.

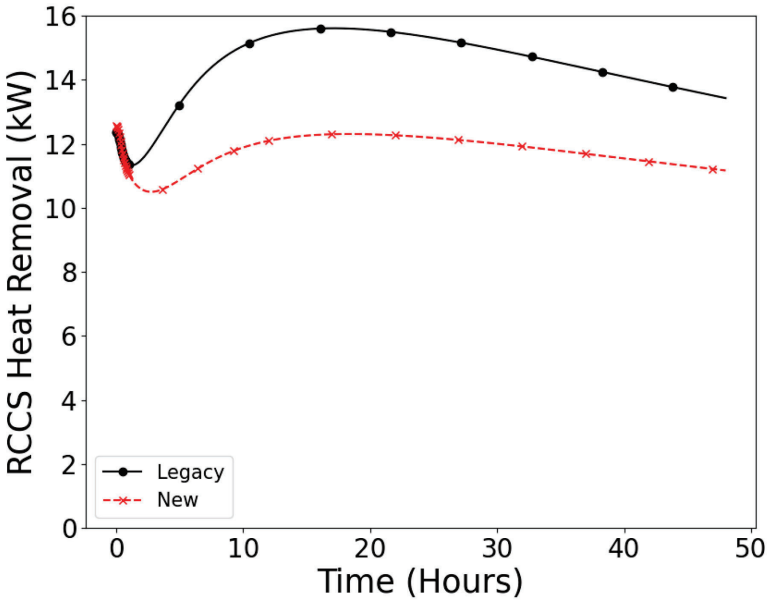

Figure 35. RCCS heat removal rates during the PCC.

Table 4. Comparison of minimum RCCS heat removal rates (kW).

Transient	Legacy Model	New Model
DCC	10.10	8.20
PCC	11.33	10.50

Greater heat removal in the PCC than the DCC is a result of natural circulation in the PCC. In the inner reflector, inner core, and middle core, helium reverses flow and rises. The helium mixes in the upper plenum, imparting some energy on the upper head of the vessel. The helium then falls and flows downward through the outer core and the outer reflector flow channels. This transfers heat from the inner regions of the core and the inner reflector to the outer core and outer reflector, effectively reducing the thermal resistance between the inner and outer portions of the facility. The natural circulation flow rate was calculated by summing the flow of the outer core and outer reflector regions, as these regions are both in downflow and represent the entire downflow region. In the legacy model, the natural circulation flow rate was 0.30 g/s and in the new model, the natural circulation flow rate is 0.24 g/s. The flow rates in each region can be seen in Figure 36. Comparing just the flow rate at 48 hours shows that the natural circulation flow in the new model is only 80% that of the flow rate in the legacy model. In isolation, this seems like a large difference in flow rates; however, considering that the natural circulation flow rate is a fraction of a gram per second, and the full-power flow rate is 1 kg/s, the difference amounts to approximately 0.6% of the nominal flow rate. The patterns in both space and time shown in Figure 36 are similar but not the same. The flow rate should not evolve in exactly the same way, because the new model represents the core with a finer discretization and captures the hydraulic diameter of the rings with a mix of coolant channel sizes differently than the legacy model does. Overall, the agreement in natural circulation between the two models is quite good.

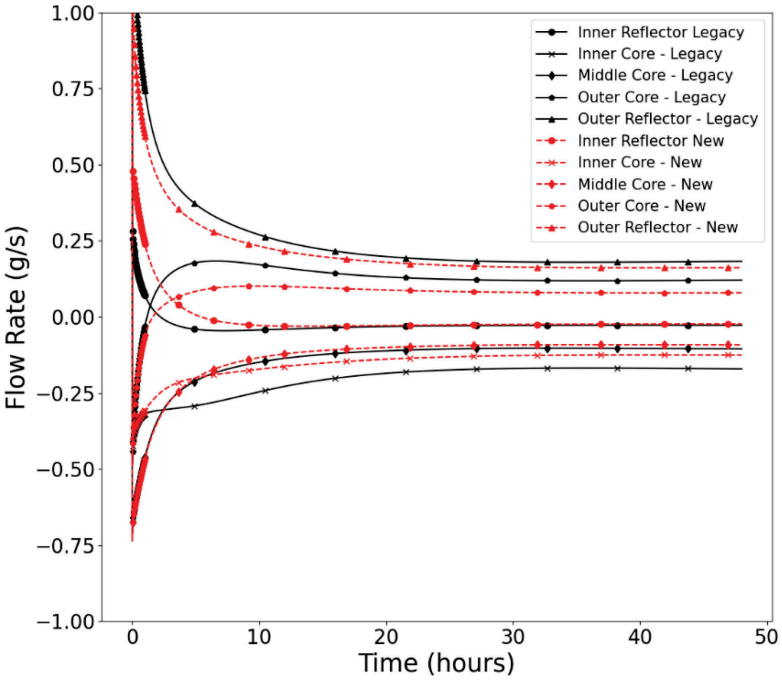

Figure 36. Natural circulation flow rates in the PCC.

3.2.3 Problem 3 Exercise 1C

P3Ex1C represents a low-power steady state similar to the extended steady state in PG-27. The boundary conditions for P3Ex1C are shown in Table 5. The heat generation for this exercise is split between the middle and outer rings of the legacy model in a 9.5/90.5% split [14]. In the new model, the heat is generated in Rings 7 and 8 (where Ring 1 is the first ring containing heater rods). This very local heat generation is exactly the type of scenario the new model was built for. The improved resolution of the new model better captures the radial temperature variation within the core.

Table 5. Boundary conditions for P3Ex1C.

Parameter	Value
Power (kW)	86.0
Helium Mass Flow Rate (kg/s)	0.1
Helium Inlet Temperature (K)	380.0
Helium Pressure (MPa)	0.13
RCCS Water Mass Flow Rate (kg/s)	0.33
RCCS Water Inlet Temperature (K)	313.2
RCCS Water Pressure (MPa)	0.1
RCCS Cavity Air Flow Rate (kg/s)	0.025
RCCS Cavity Air Inlet Temperature (K)	300.0

The energy balance comparison between the new and legacy models for P3Ex1C is shown in Table 6. We see that the primary helium and air in the RCCS cavity remove more energy in the new model than in the legacy model while the RCCS removes less energy in the new model. Ex1A also showed that heat removal by convection in the core was greater in the new model than in the legacy model. Table 7 shows the comparison of flow rates between the two models for P3Ex1C. The bypass flow fraction in the legacy model is 11.96%, and in the new model, it is 11.69%. The difference in bypass flow, and the difference between flow rate in any region of the core is below 5% of the average between the two models.

Table 6. Energy balance in P3Ex1C.

Region	Fluid	Outlet Temperature Legacy/New (K)	Difference (K)	Power Removed, Legacy/New (kW)	Difference (kw)
Reactor Vessel	Helium	537.6/538.7	1.1	81.97/82.65	0.68
RCCS Panels	Water	315.1/314.8	-0.3	2.63/2.18	-0.45
RCCS Cavity	Air	331.3/334.3	3.0	0.50/0.69	0.19

Table 7. Mass flow rate distribution in P3Ex1C.

	Inner Reflector	Inner Core	Middle Core	Outer Core	Outer Reflector
Legacy Model Flow Rate (kg/s)	0.0031	0.02596	0.0335	0.0286	0.0089
New Model Flow Rate (kg/s)	0.0032	0.0247	0.0351	0.0285	0.0085
Difference (kg/s, New - Legacy)	1.15e-4	-1.21e-3	1.66e-3	-1.71e-4	-3.93e-4

The block temperatures in the new model show generally lower temperatures in the inner reflector and most of the core, but in the outer core region, where the heat is generated, the block temperature is generally higher, except for the temperature at the top of the lower reflector, as shown in Figure 37. Temperatures in the permanent reflector are generally higher in the new model than in the legacy model. Temperatures at Block 9 show an unexpected temperature rise moving from the outer reflector towards the permanent reflector, from radial positions of approximately 0.5–0.6 m. This result requires further investigation.

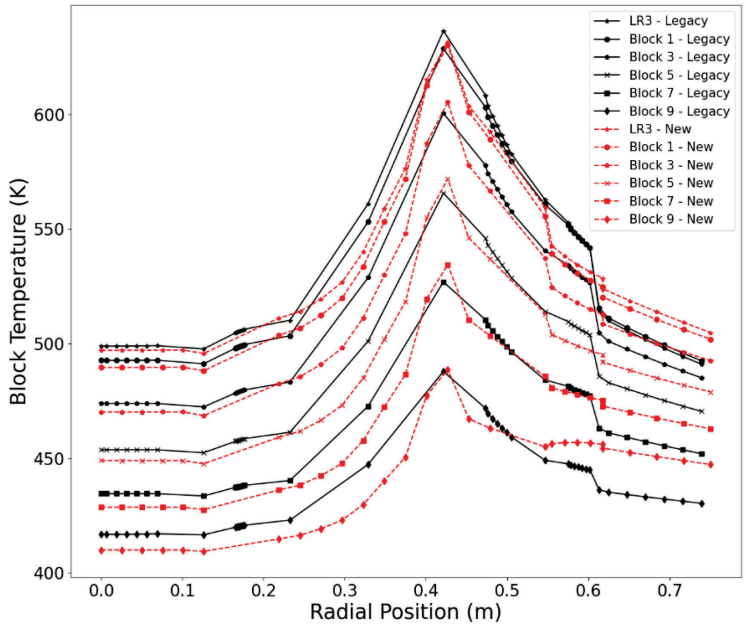

Figure 37. Block temperature distribution in P3Ex1C.

The helium temperature distribution can be seen in Figure 38. Helium temperatures show some unexpected trends. The fact that the temperature in Ring 0 of the new model, at a position just above 0.2 m, is higher than the temperatures on either side of it, is an unexpected result that requires further investigation to understand. Notably, the block temperatures in Figure 37 do not show higher Ring 0 temperatures for the block, so this unexpected result is not driven by unexpected block temperatures but likely arises due to either flow rate distribution, differences in heat transfer coefficient and the corresponding ΔT between block and coolant, or some combination of both. The helium temperature in the outer core, where most of the heat is generated, is generally lower in the new model than the legacy model. At Block 9, the helium temperature is highest in the outermost ring, which is not the expected result. The behavior at Block 9 is also unexpected for block temperature. This anomalous behavior at Block 9 requires further investigation.

Figure 39 shows the core barrel and vessel temperatures during the steady state. These results indicate that the thermal resistance between the reflector and barrel is higher in the new model than in the legacy model. The lower temperature of the vessel in the new model contributes to the lower heat removal by the RCCS, because radiation heat transfer scales with the fourth power of temperature, and the temperature is lower in the new model. The shape of the barrel and vessel temperatures in the same in both models.

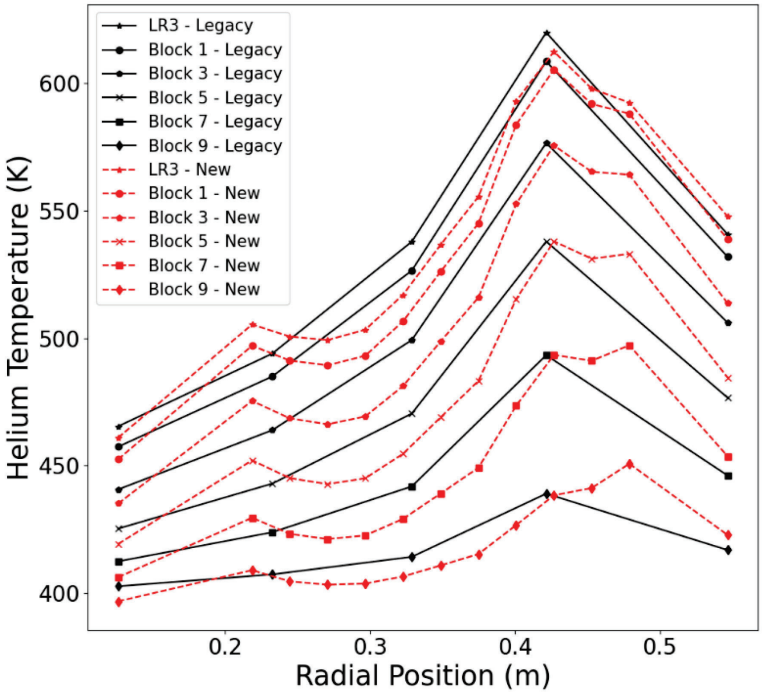

Figure 38. Helium temperature distribution in P3Ex1C.

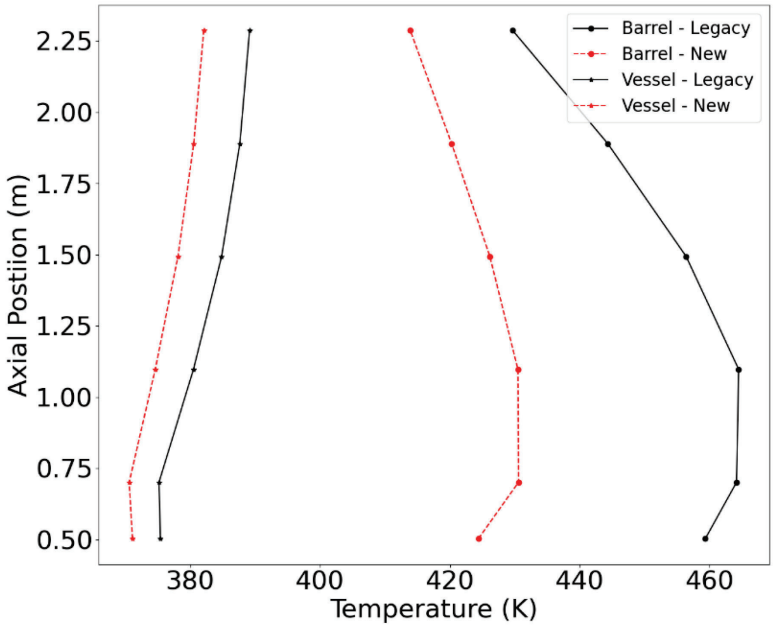

Figure 39. Core barrel and reactor vessel temperatures in P3Ex1C.

Generally, results from the new model show similar trends to the legacy model but with a greater resolution. P3Ex1C and P3Ex1D are more representative of the conditions for which the new model was developed. The finer resolution in temperatures highlights the value of the new model, but temperatures at Block 9 require further investigation.

3.2.4 Problem 3 Exercise 1D

P3Ex1D represents a simplified version of PG-27. The primary coolant flow rate is reduced from 0.1 to 0.0 kg/s linearly in the first 1.0 seconds. The coolant outlet pressure remains unchanged, as do pressures and flow rates in the cavity and RCCS. The power versus time curve is shown in Figure 40. The transient is run out to a time of 48 hours, but after 4 hours, the power is turned off for the remainder of the exercise. Coolant flow rate over time is a figure of merit in this exercise, but we will not present it in this section of the report, because the natural circulation flow rates are on the order of 3–5 micrograms per second. This is a negligible flow rate in both models, so we will not discuss it further. Natural circulation is generally not an important phenomenon in HTTF due to the low operating pressure relative to HTGRs.

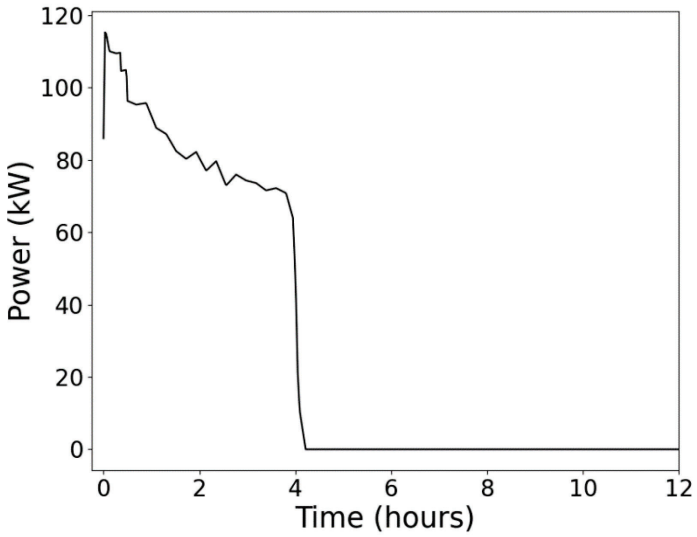

Figure 40. Power versus time in P3Ex1D.

Temperatures plotted versus time show a similar trend in P3Ex1D as is seen when P2Ex1B and P3Ex1B results are compared between models. The new model experiences a much slower long-term cooldown than the legacy model. The benchmark specifications for P3Ex1D request block and helium temperatures at every radial TC position shown in Figure 1, with the note that only one block temperature can be provided for TCs at Positions 15, 16, and 17.

Figure 41 shows the temperatures at TC Position 1, the center of the facility, during P3Ex1D. In the legacy model, temperatures peak somewhere between 6 and 8 hours, depending on axial position. In the new models, temperatures peak between 10 and 13 hours depending on axial position. In both models, the peak temperature occurs well after the power is shut off but given that heat needs to conduct from the core region to the inner reflector, temperatures in the inner reflector peaking later than in the core is an expected result. A result that arises in Figure 41 that is less clear, though still present in results from Ex1B, is that temperatures in the new model converge towards a single value more quickly than the legacy model. This is likely clearer in P3Ex1D because the heat generation is turned off after 4 hours, allowing the convergence more rapidly. This likely also happens faster due to the more significant natural circulation in P2Ex1B. Temperatures at TC Position 2 are very similar to those at Position 1. Figure 42 shows block temperatures at TC Position 5 during P3Ex1D. For all blocks shown beneath Block 9, block temperatures reach larger peaks in the new model than the legacy model. In both the new and legacy models, the block temperature peaks shortly after the power is turned off. In the new model, temperatures peak at approximately 4.5 hours, and in the legacy model, it is at approximately 5 hours. Once again, block temperatures in the new model converge more rapidly than those in the legacy model.

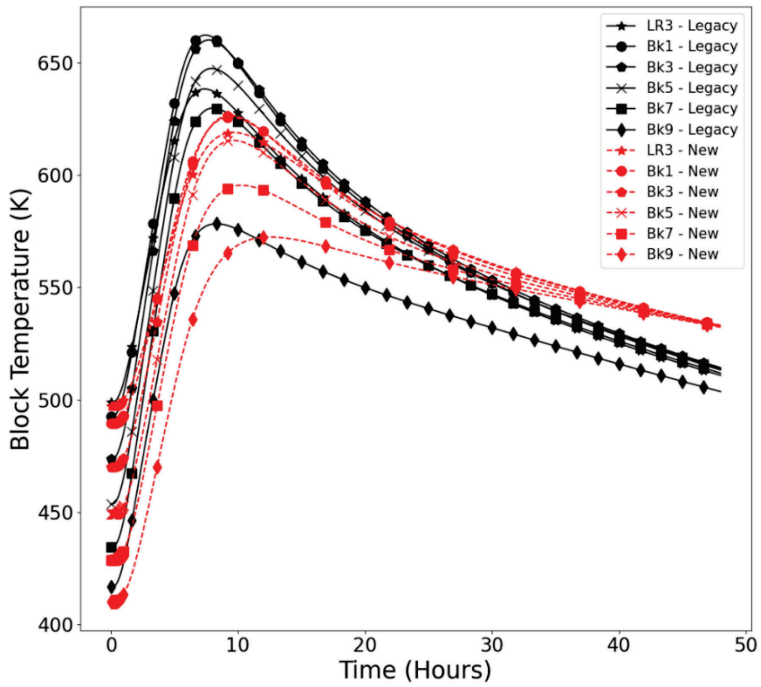

Figure 41. Temperatures at the center of the inner reflector during P3Ex1D.

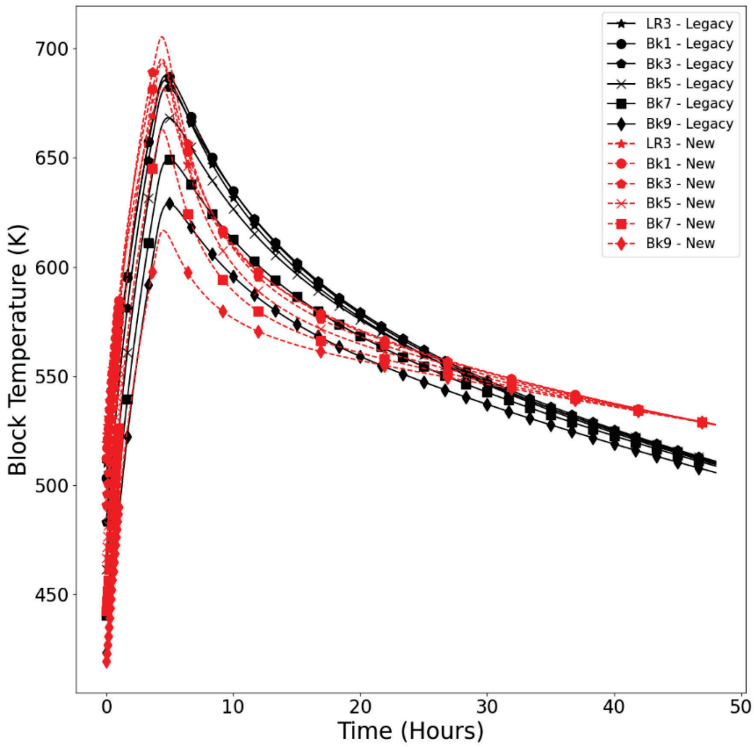

Figure 42. Block temperatures at TC Location 5 during P3Ex1D.

Helium temperatures at TC Location 6 show essentially the same results as block temperatures at Location 5. Additionally, Locations 7 and 8 are quite close to Locations 5 and 6, so results from those blocks are not shown. The heat in this exercise is generated in heater rods near TC Locations 9 (block) and 10 (helium). In both models, block temperatures peak at 4 hours, or shortly before 4 hours near the bottom of the core. In the legacy model, the highest temperature is reached in Block 1, but in the new model, it is reached in Block 3. This, combined with temperatures converging more rapidly in the new model, suggests that axial conduction is a more significant effect in the new model than the legacy model. In the new model, peak temperatures are higher than those in the legacy model at Blocks 1, 3, 5, and 7, whereas peak temperatures at LR3 and Block 9 are lower in the new model than the legacy one. The initial cooldown following shutdown at 4 hours is more rapid in the new model, but by 30 hours, temperatures at this radial position in the new model are higher at all axial locations than in the legacy model. These results can be seen in Figure 43. Helium temperatures shown in Figure 44 show the same behavior as block temperatures in this region.

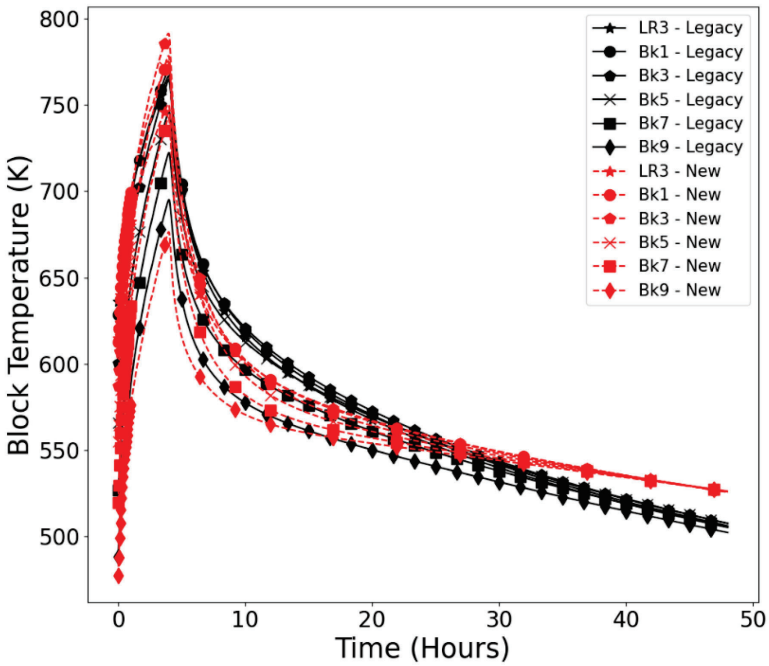

Figure 43. Block temperatures at TC Location 9.

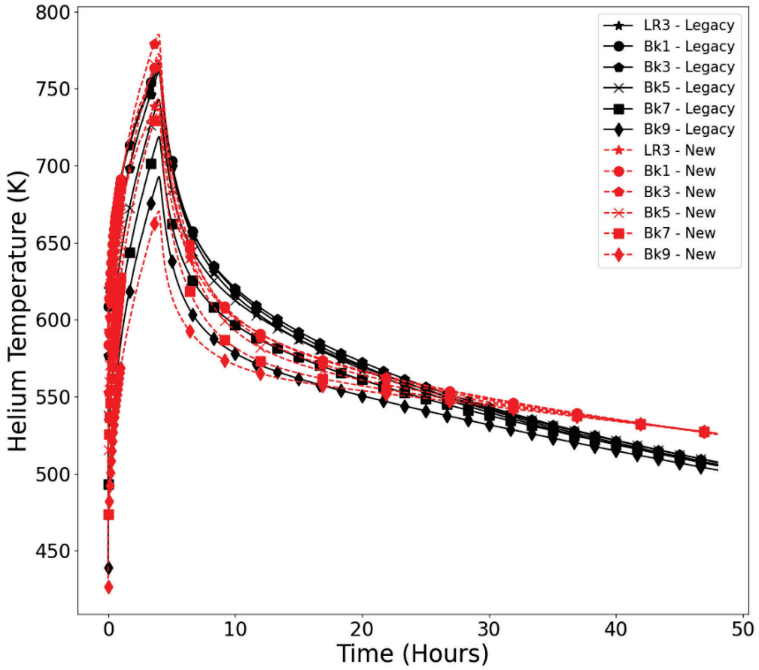

Figure 44. Helium temperatures at TC Location 10.

Temperatures in the outer reflector can be seen in Figure 45 and Figure 46. Peak temperatures are lower in the new model at both locations. At Location 14, the temperature rise is lower in the new model than the legacy one. At TC Location 15, the temperature rise from steady state to peak is higher in the legacy model at all axial locations except at Block 9. Figure 46 shows that the temperature rise at Block 9 is slower in the new model than the legacy one. We once again see that the long-term cooldown is much slower than in the legacy model.

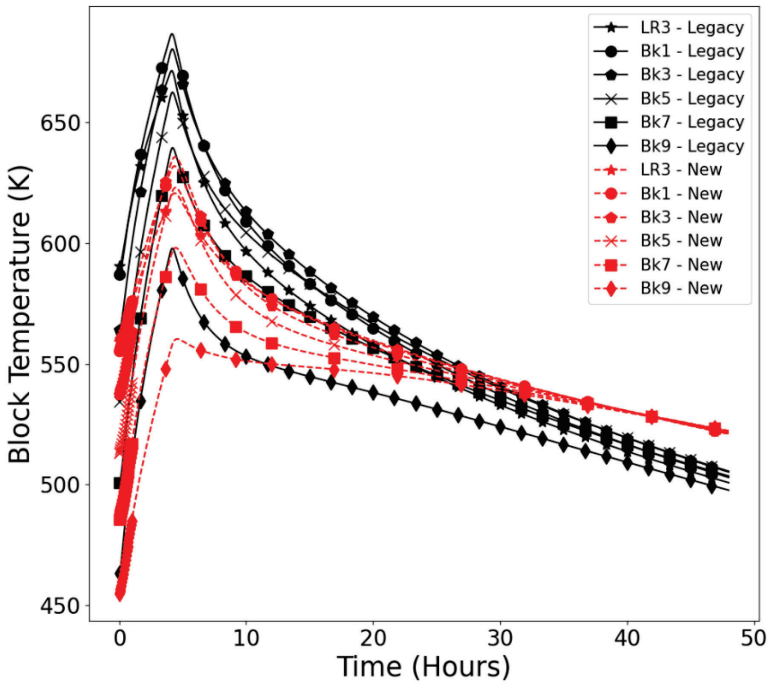

Figure 45. Temperatures at TC Location 14.

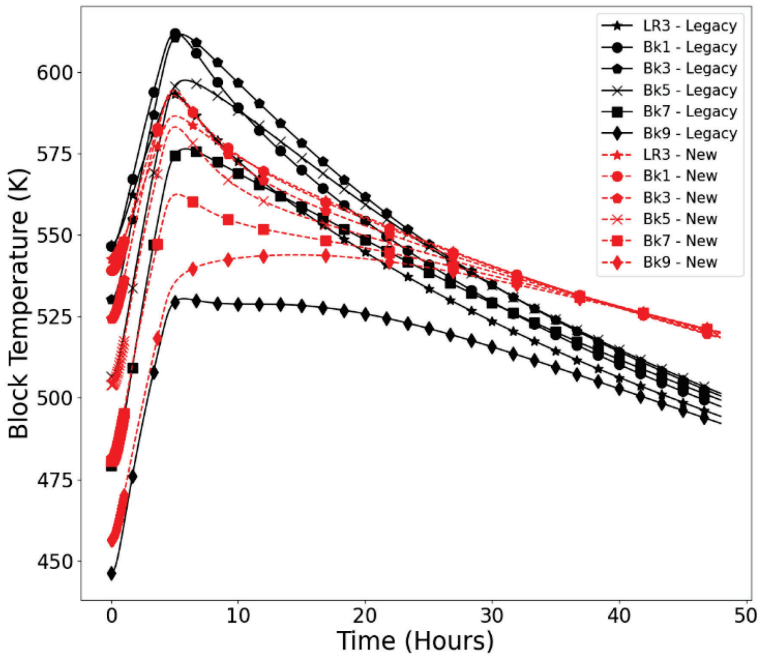

Figure 46. Block temperatures at TC Location 15.

Temperatures in the PSR over time can be seen in Figure 47. The temperature rise in the new model is slower and lower than in the legacy model, and once again, the long-term cooldown is slower in the new model than the legacy model.

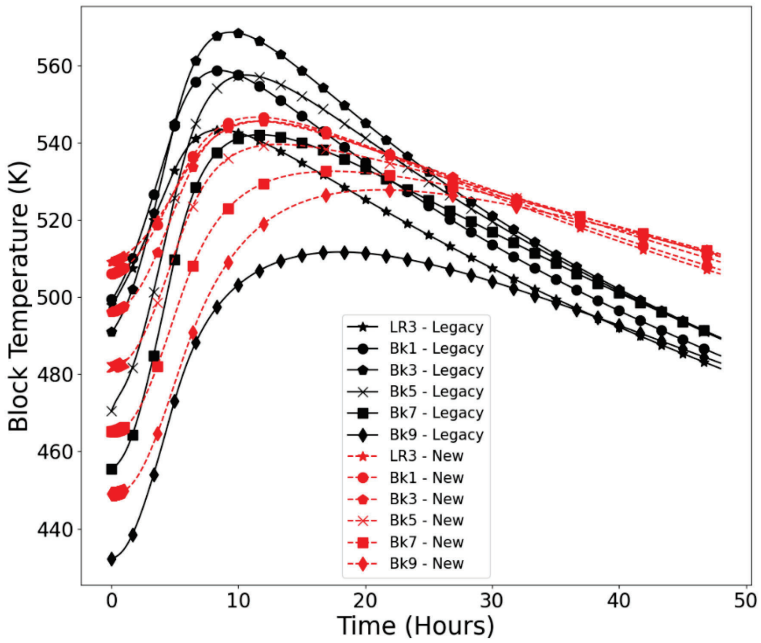

Figure 47. Temperatures at TC Location 18.

Table 6 shows that the heat removal by the RCCS is lower in the new model than the legacy one in steady state. This provides some explanation for the lower long-term heat removal. Figure 48 shows that the RCCS heat removal is lower in the new model during the entire 48 hours modeled. The RCCS itself was not changed between the new and legacy models, so only changes within the core and the PSR can explain the difference in RCCS heat removal. These results show that the thermal resistance between the core and RCCS is greater in the new model than the legacy one.

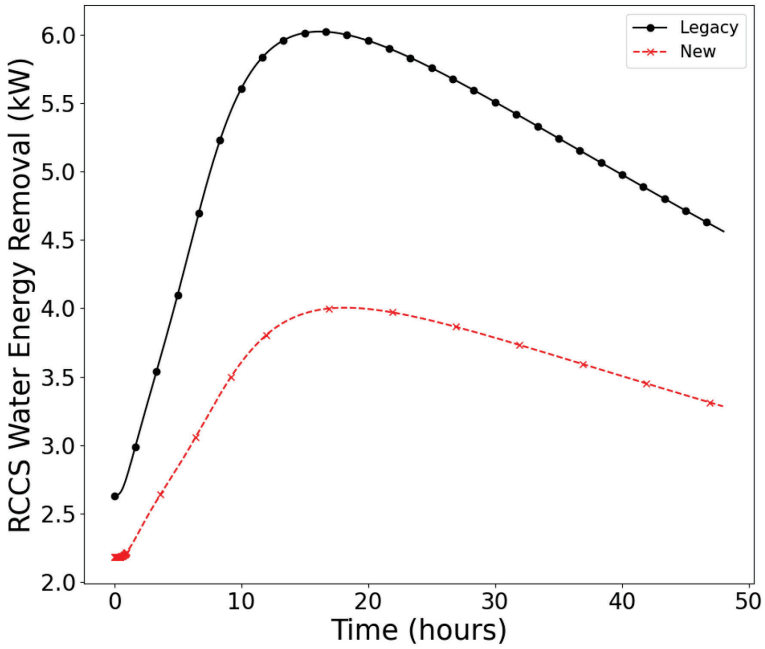

Figure 48. RCCS heat removal in P3Ex1D.

P3Ex1D is an azimuthally symmetric transient with significant radial heat generation variations. This makes it a valuable example of the capabilities of the new model. In the core, temperatures change more rapidly in the new model than the legacy one, but temperatures in both reflectors generally rise slower and to lower peak temperatures. P2Ex1B and P3Ex1B show a slower long-term cooldown in the new model than in the legacy model, which is also shown in P3Ex1D. This could be driven by changes in the conduction enclosures, but it may also be a result of the change from a radiation enclosure between the outer reflector and the PSR to a conduction enclosure in the new model.

4. RELAP5-3D VALIDATION STUDIES WITH THE NEW MODEL

In Section 3, we discussed results from P2Ex1 before P3Ex1. Here, we will discuss results from P3Ex2 before we discuss P2Ex2. This is because the extended steady state in PG-27 makes it possible to perform some calibration studies for the steady state and to test that calibration on the PG-27 transient data followed by the PG-29 data, which are all transient data. As such, presenting the calibrations from P3Ex2 is required before they can be appropriately discussed in the context of P2Ex2. This work is essentially a replication of the validation analysis performed by Kile et al. [14] but using the new model instead of the legacy model.

4.1 Problem 3 Exercise 2

4.1.1 Steady-State Calibration

This analysis is based on HTTF experiment PG-27. The PG-27 experiment represents a PCC. The power in PG-27 is generated in the outer regions of the core, as shown in Figure 49. The experiment consists of three distinct phases: a heat up, a long-term low-power steady state, and the PCC. The PCC portion of the experiment includes a dramatic jump in power followed by a decay of the power along a scaled MHTGR-350 decay heat curve.

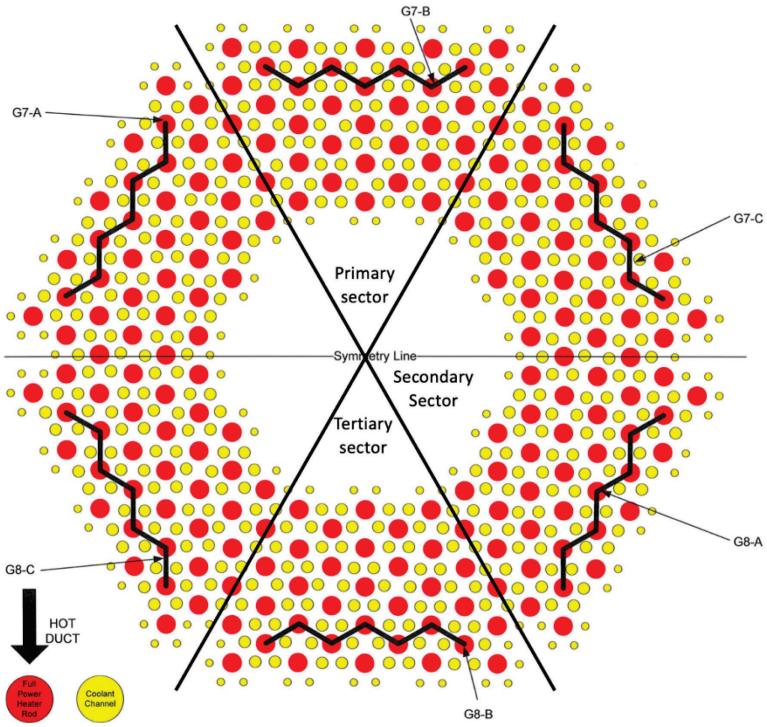

Figure 49. PG-27 active heater rod distribution. Active heaters are the red circles connected by black lines. Reproduced from Reference [14].

As mentioned, we will first discuss P3Ex2 as PG-27 consists of an extended steady-state period. We will take advantage of this extended steady state to investigate potential adjustments to the new model. The primary tuning made to the new model was the adjustment of the effective thermal conductivity (ETC) of the core block structural material Greencast-94F. This calibration assumed that the ETC of the blocks would be 34% of the measured value, taking into account the holes in the blocks for heater rods and coolant channels, as well as any potential cracks or other types of damage in the blocks [14]. This 34% was found to be an optimal calibration when comparing the legacy model to experimental data in the sensitivity studies done in [14]. The calibrated ETC will be implemented into the extended steady-state model to compare to the noncalibrated model and the experimental steady-state data. This will help demonstrate whether the ETC improves the results of the new model, which will then be applied to the transient testing for PG-27 and later for PG-29 in P2Ex2.

To simulate the PG-27 extended steady state in the new model, initial conditions and boundary conditions were extracted from the PG-27 experimental data. The key boundary conditions included the primary coolant inlet temperature, primary coolant outlet pressure, total heater rod power, RCCS inlet temperature, and RCCS inlet mass flow rate. The initial conditions included the initial temperatures of the core structures, primary coolant throughout the core, and heater rod initial temperatures. The sensors that captured the data for the aforementioned conditions were identified using the HTTF instrumentation plan [15]. Malfunctioning and other excluded sensors were identified in the Oregon State University HTTF PG-27 test acceptance report; these were not included in the implementation of boundary and initial conditions. For the time-dependent boundary conditions, the data had to be smoothed to reduce noise from the sensors; this was done using a simple moving average. In addition, during the smoothing, the number of representative data points was reduced to fit within limits of the RELAP5-3D input file. The experimental start time for the steady state was found to be 60 hours (216,000 seconds), the time prior to this point was the heat-up period for the system. The conditions at t=216,000 seconds were populated into the new RELAP5-3D model and the model was allowed to run until the RCCS coolant temperatures

converged, which took about 60,000 seconds. The steady-state RCCS temperature data from PG-27 converges to about 297 K before the onset of the PCC. The RELAP5-3D model appears to be overpredicting the RCCS temperature by a substantial amount (>25 K) compared to the experimental data. This can be indicative that too much heat is being removed from the core in the RELAP5-3D model, prompting the need for further investigation in the future.

We also compared radial temperature distribution between models and experimental data. Figure 50 shows the temperatures at different normalized radial points for Blocks 3, 5, and 7. All temperatures from the new model are taken from the primary sector, but all sectors in the new model provide temperature readings that are essentially identical. Differences arise due to slight variations in power between the G7 and G8 banks in Figure 49, but these differences are insignificant. These results demonstrate that the calibrated ETC model improved agreement over the nominal model. Specifically, the ETC model shows excellent agreement to the data for the inner cylinder and reflector and across the inner, middle, and outer core. The model begins to underpredict temperatures in the outer reflector and outer shell regions, particularly in the lower axial positions, but still demonstrates reasonable agreement with the data.

Figure 51 shows a direct comparison of the new and legacy ETC models against the data. The new model clearly performs better in most areas. Only the outer reflector has temperatures that are predicted worse by the new model. Temperatures in the PSR are lower in the new model than the legacy model, but they are still within the spread of the measured data, so these lower temperatures are not considered "worse". Overall, this analysis shows that steady-state temperatures are significantly improved in the new model. Note that in both Figure 50 and Figure 51, there are data points missing for TC location 9 in the secondary sector at block 7 and the tertiary sector at block 3. The line passing through TC location 9 should not be considered as a predicted or measured temperature at TC location 9 in that sector.

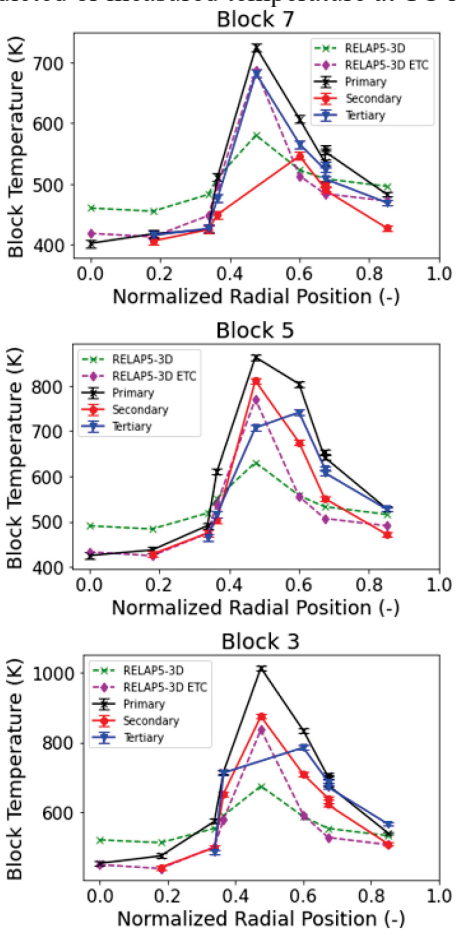

Figure 50. Steady-state radial temperature distributions in the new model with and without the ETC.

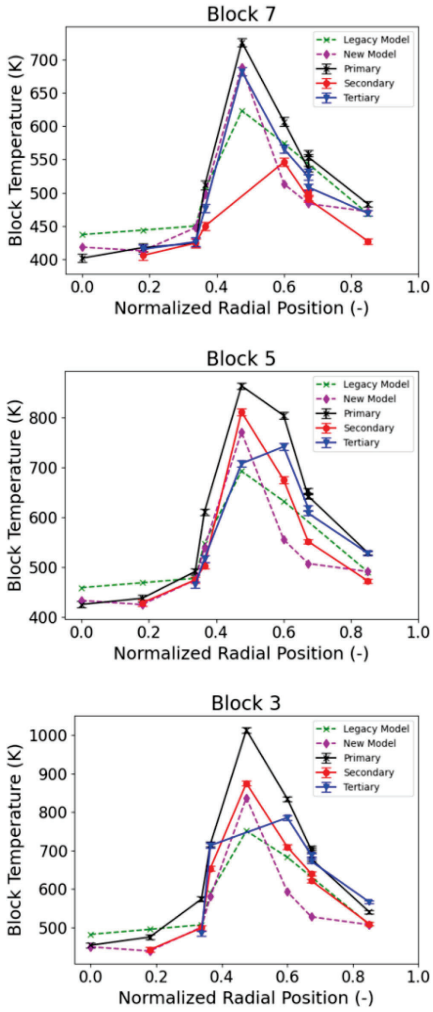

Figure 51. Comparison of best-estimate (ETC) models of the new and legacy models.

4.1.2 Transient Testing

The steady-state conditions from the previous section were used as the initial conditions for the PG-27 transient. Once again, two versions of the new model were used. One used the measured thermal conductivity of the Greencast-94F material, while the other used the ETC of 34% of the measured thermal conductivity. This provides us an opportunity to determine if the calibration leads to improved results when compared to the experimental data. Based on the steady-state results, we expected the ETC model to show better agreement during the transient than the nominal thermal conductivity model. For the transient testing, the system was in steady state until 5 hours, with the PCC beginning between roughly 6 and 7 hrs. Figure 52 shows the temperature comparison between the PG-27 data and the nominal and ETC models for the central cylinder of the inner reflector. Both versions of the RELAP5-3D model significantly underpredict the temperature rise in this region, with the nominal version having superior agreement over the ETC with respect to capturing the trend. The ETC model appears to lag the pace of the experimental data, indicating a potential issue with the thermal conductivity of the central cylinder or conductance model. Similar behavior can be seen in the inner reflector region in Figure 53. The predicted results for both the inner cylinder and inner reflector are considered to be in minimal agreement for the nominal model and insufficient agreement for the ETC. A common pattern is that the ETC model begins

to demonstrate stronger agreement to the data as the normalized radius approaches the active heated region.

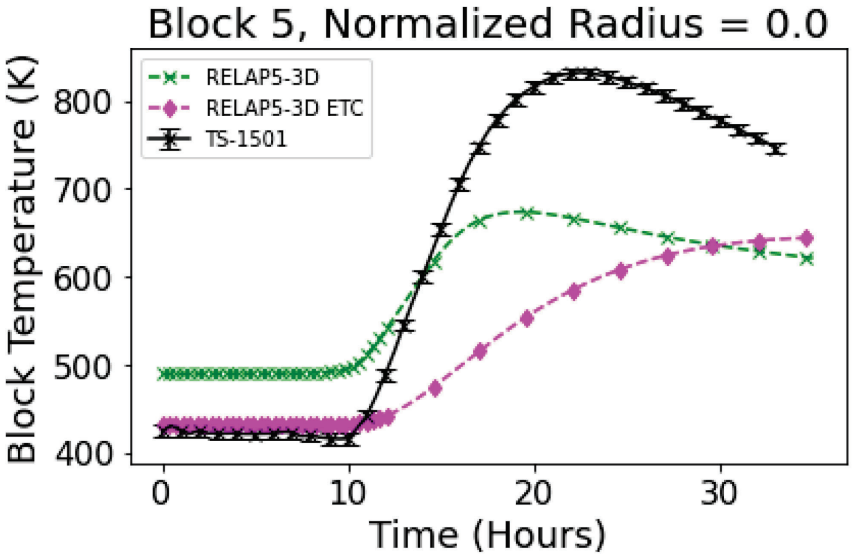

Figure 52. Temperature comparison of the inner reflector central cylinder.

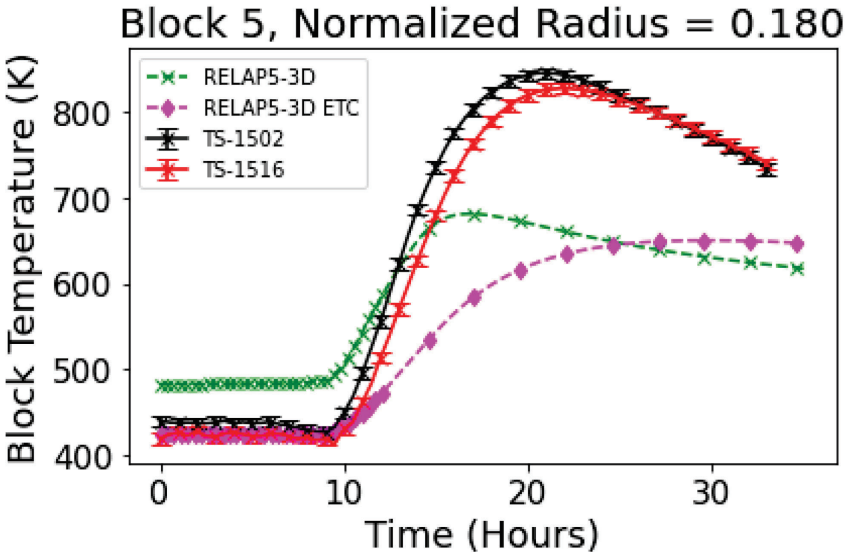

Figure 53. Temperature comparison across the inner reflector.

The next section focuses on the temperature of the core regions. Figures 54–56 depict the comparisons for the inner, middle, and outer core regions, respectively. Once again, all RELAP5-3D temperatures come from the primary sector. In Figure 54, the ETC model begins to better represent the experimental data by a small margin over the nominal model. The trend is well predicted, but there is still a large discrepancy (200 K) in the peak temperature rise, demonstrating minimal agreement. Figure 55 demonstrates further improvement for the ETC model with the trend and peak temperature rise, with a peak discrepancy of about 150 K. Both versions of the model would still be categorized as minimal agreement, but the difference between the ETC and nominal models has increased in favor of the ETC. Lastly, Figure 56 depicts the outer core, which is the active heated region for PG-27. The ETC model shows significantly improved agreement over the nominal model with respect to the peak temperature rise, narrowing the underprediction of the temperature to less than 100 K. The ETC model demonstrates reasonable agreement for the outer core region. The key takeaway from the core region is that the ETC model outperforms the nominal model in regions closer to the active heaters.

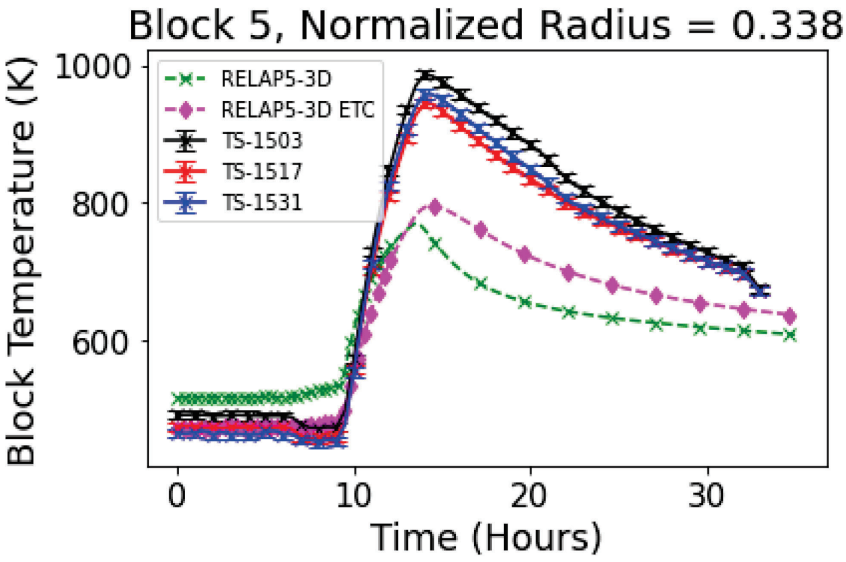

Figure 54. Temperature comparison for the inner core.

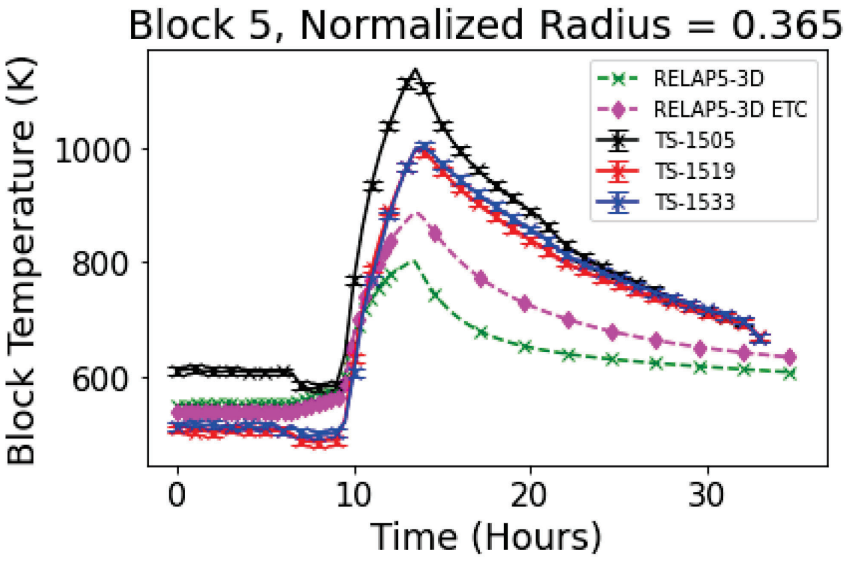

Figure 55. Temperature comparison for the middle core.

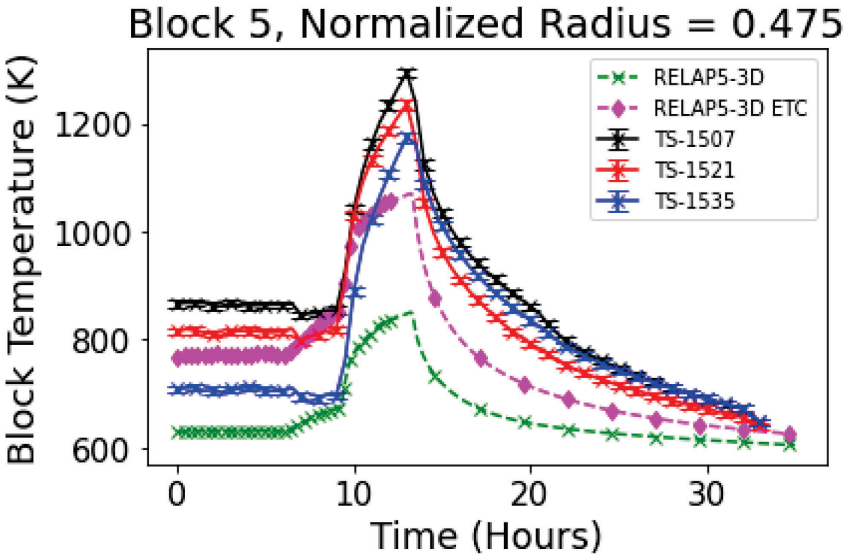

Figure 56. Temperature comparison for the outer core.

The third main region includes the outer reflector, outer shell, and PSR. Figure 57 displays the temperature behavior in the outer reflector. Both versions of the model are predicting similar results, both of which are significantly underpredicting the measured temperature. The magnitude of the change in temperature is underpredicted by over 200 K, demonstrating insufficient agreement for both models. Likewise, Figure 58 depicts the temperature in the outer shell region of the outer reflector. The nominal model begins to outperform the ETC model by a notable margin. However, the nominal model still underpredicts the experimental data by 200 K; both models still display insufficient agreement in this region. Figure 59 shows the temperature in the PSR. The nominal model is still outperforming the ETC model in capturing the temperature trend and rise; it underpredicts the peak temperature rise by approximately 50 K, demonstrating reasonable agreement. The ETC model is underpredicting by over 75 K, demonstrating minimal agreement.

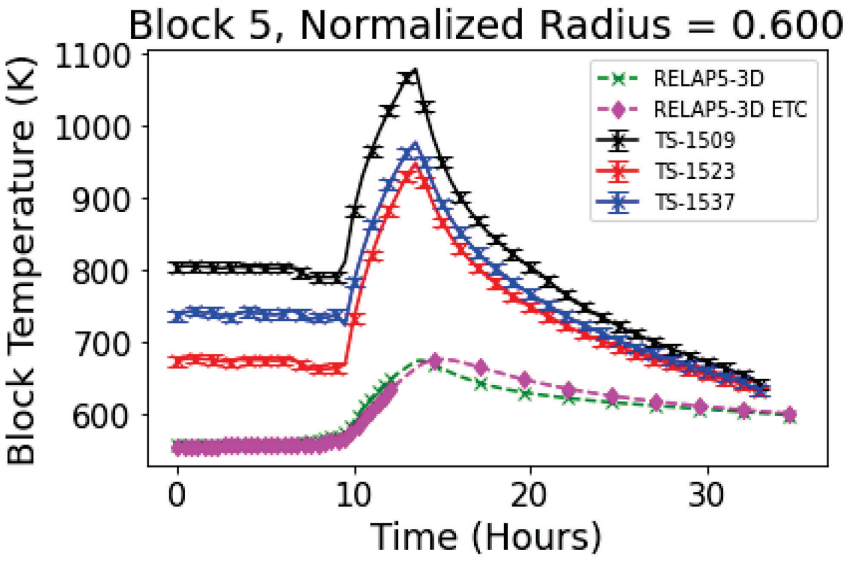

Figure 57. Temperature comparison for the outer reflector.

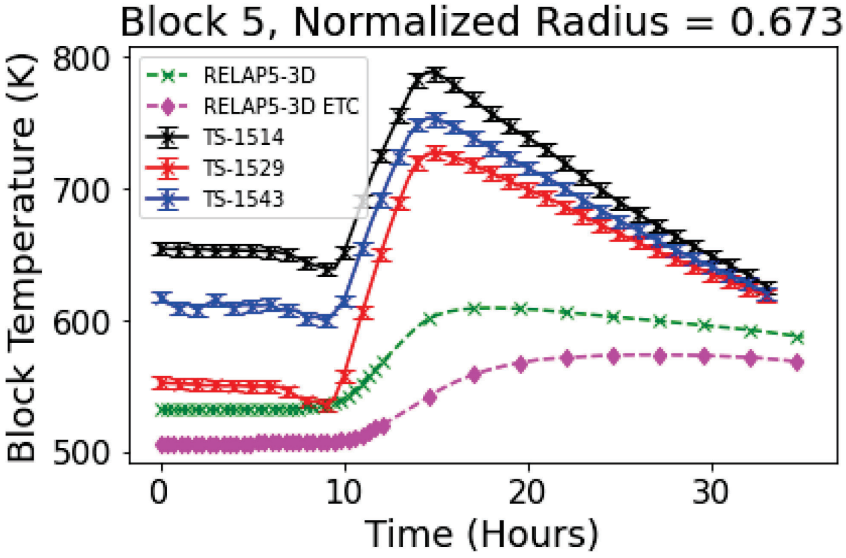

Figure 58. Temperature comparison for the outer shell.

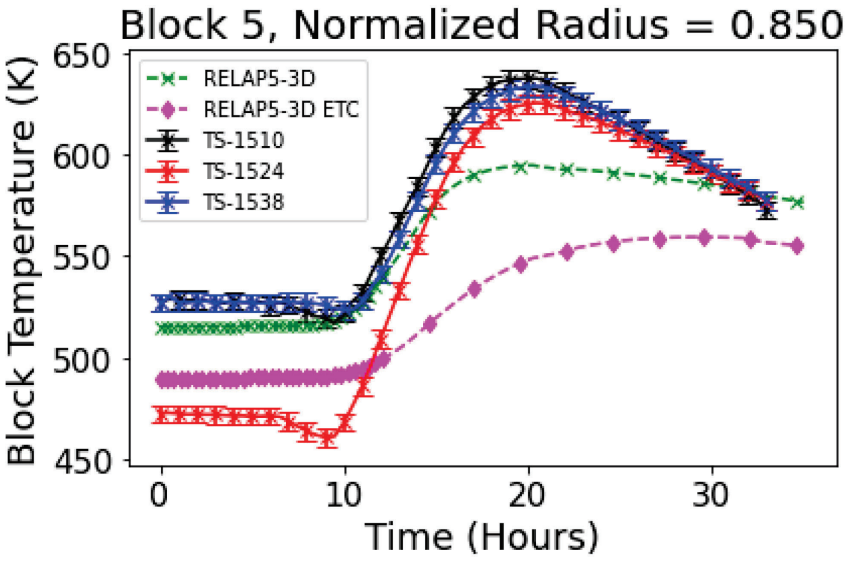

Figure 59. Temperature comparison for the PSR.

Finally, Figure 60 shows the RCCS coolant outlet temperature throughout the transient. For both models, there is excellent agreement at the onset of the PCC. However, at about t=13 hours, both models begin to diverge from the experimental data and the temperature trends upward, while the experimental data displays a decrease over time. By the end of the transient, both models are overpredicting the RCCS outlet temperature by over 50 K. This behavior can be indicative that too much heat is being transferred to the RCCS in the RELAP5-3D model. This overprediction of the temperature and failure to properly predict the temperature trend demonstrates that both models have insufficient agreement.

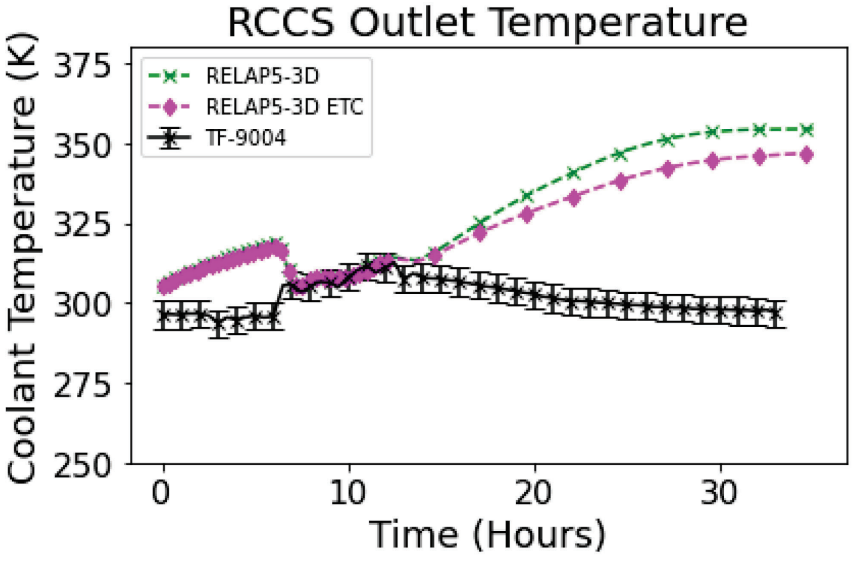

Figure 60. RCCS coolant outlet temperature.

This analysis has shown that, in the core, the ETC models better predict block temperatures than the nominal models, but in the reflector regions, produce a worse outcome. This is to be expected, because the relative degradation of thermal conductivity in the reflectors should be much lower than in the core, but we used the ETC everywhere. A future model will use the ETC only within the core regions and will use the bulk Greencast-94F thermal conductivity. The best-estimate legacy model used the ETC

everywhere as well. Comparison of temperatures in the inner reflector central cylinder between the new and legacy models can be seen in Figure 61. The new model predicts a much slower temperature rise in the inner reflector than the legacy model does, despite predicting a better steady-state temperature. Figure 62 shows that the block temperatures predicted by the new model in the outer core are in better agreement with measured values than those predicted by the legacy model until the heaters are shut off at approximately 14 hours. The cooldown in the new model is faster than the legacy model, but the core temperatures are generally better predicted.

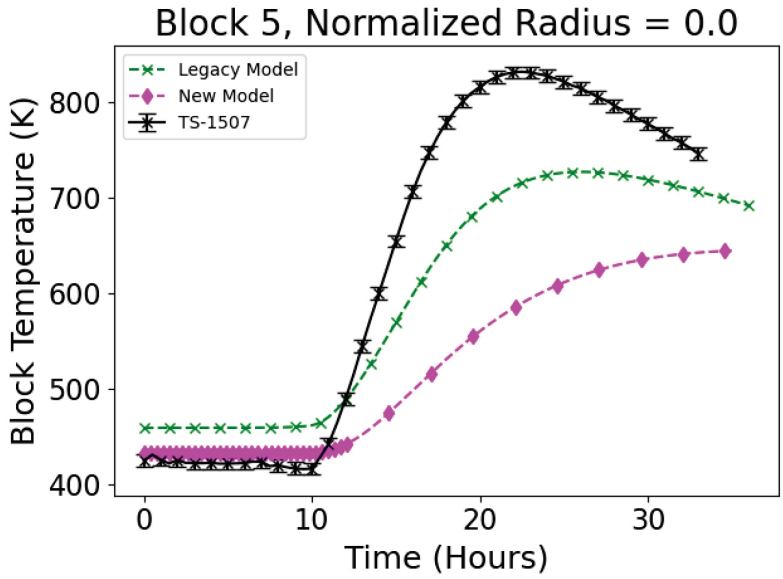

Figure 61. Inner reflector central cylinder temperature comparison between the new and legacy models

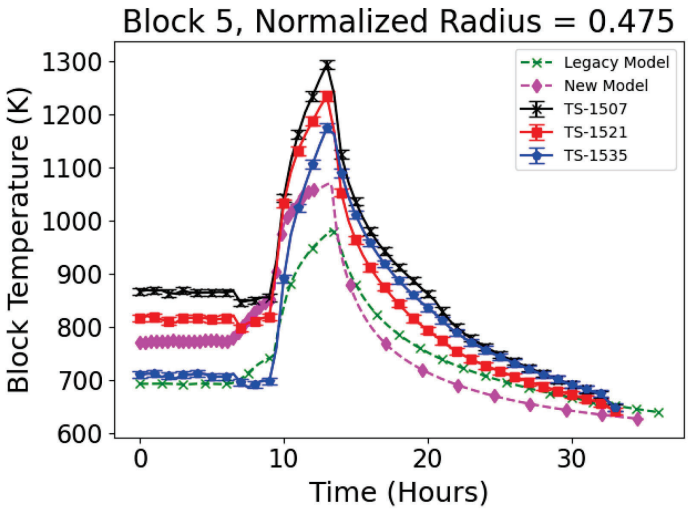

Figure 62. Block temperatures at TC position 9 during the experiment and predicted by the new and legacy models

The transient temperature rise, defined here as the difference between the maximum temperature and the initial temperature, can be seen in Table 8. The temperature rise from the data is defined as the average rise from TCs in each sector. At block 7, the temperature rise in the new model is smaller than the one in the legacy model. At blocks 3 and 5, the temperature rise is slightly higher, except for the inner ring of block 5, where the temperature rise is slightly lower in the new model. The difference in

temperature rise between the new and legacy models is relatively small. The largest difference is 20 K. This suggests two things: Firstly, the improved prediction shown in Figure 62 is largely a function of the higher initial temperature. Secondly, the hypothesis that the new model would improve temperature rise may be incorrect. Additional investigation into heat removal may be required to assess this hypothesis more completely.

Table 8. Temperature rise (K) comparison between the Data|Legacy Model|New Model

	Inner Ring	Middle Ring	Outer Ring
Block 7	480|336|316	552|349|342	505|327|322
Block 5	487|326|323	504|330|348	453|289|301
Block 3	424|311|313	426|308|327	322|256|258

4.2 Problem 2 Exercise 2

The PG-29 experiment represents an asymmetrically heated DCC. PG-29 was performed immediately following the PG-28 experiment, which uses asymmetric heating to demonstrate hot gas mixing in the lower plenum. The distribution of active heater rods in PG-29 can be seen in Figure 64. In PG-27, we have some knowledge of the power distribution within the active heaters, because the power in the G7 and G8 banks is reported separately. In PG-29, we know which heater rods were active, but due to the hybrid heater configuration that was used, we do not know how power was distributed within those heater rods. We assume for the sake of this and previous PG-29 analysis that the power was distributed evenly among all active heater rods. We do not compare values between the new and legacy models here, because values from the legacy model have no counterpart in the multi-sector, asymmetric model and experiment in this analysis. This section demonstrates a capability developed in the new model that was not available in the legacy model.

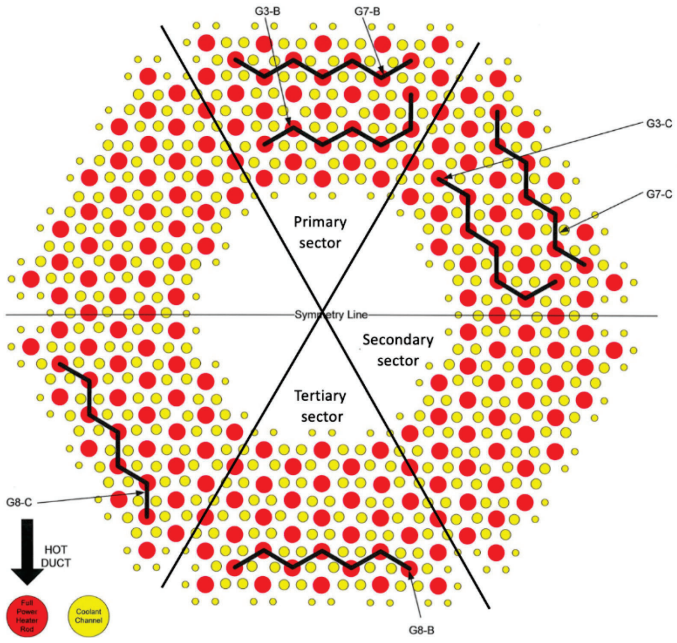

Figure 63. Active heater rod distribution in PG-29. Reproduced from Reference [14].

Due to the improved agreement seen with the ETC calibrated model, that model was also implemented for the PG-29 DCC simulation. Similar to PG-27, PG-29 quality data was selected and read for boundary conditions and initial conditions based off the PG-29 test acceptance report. This model starts approximately 5.5 hours prior to the start of the actual PG-29 test, but it is consistent with the times specified in the benchmark and used in Reference [14]. The initial conditions were taken at the experimental time of t=0 seconds since there was no preliminary heat-up period like PG-27; the DCC begins at t=28,800 seconds. The results of the PG-29 RELAP5-3D model will be compared to the experimental data to determine if the new model yields improvement over the legacy model with respect to agreement. As stated, the ETC calibrated model will also be compared to the experimental data and to the model that utilizes the nominal thermal conductivity. Figures 64–66 depict the comparisons between the experimental data, the measured thermal conductivity model, and the calibrated ETC model for each of the sectors at Ring 3 Block 7. For the primary sector seen in Figure 64, the ETC model demonstrates improved agreement over the measured thermal conductivity for the core blocks. However, the new ETC model still underpredicts the experimental data by over 300 K. Due to the trend still being captured well, the results would be considered in minimal agreement. As seen Figure 65, both versions of the new model are demonstrating similar temperature results and slightly overpredicting the experimental data. The results of the secondary sector are in reasonable agreement with the experimental data. Finally, Figure 66 depicts the result for the tertiary sector. Similar to the secondary sector, the ETC model does not vary much compared to the nominal model, with only slight improvements to the measured thermal conductivity. Both models follow the trend of the experimental data, but still underpredict the peak temperature rise by roughly 200 K, demonstrating minimal agreement. Based on these results, the ETC was found to notably approve the predicted results, particularly for locations with high amounts of heat (rings with active heater rods). Therefore, the subsequent comparisons will only focus on the calibrated ETC model and experimental results. Figure 67 consolidates the ETC comparison with the experimental data for Ring 3 Block 7 in all sectors.

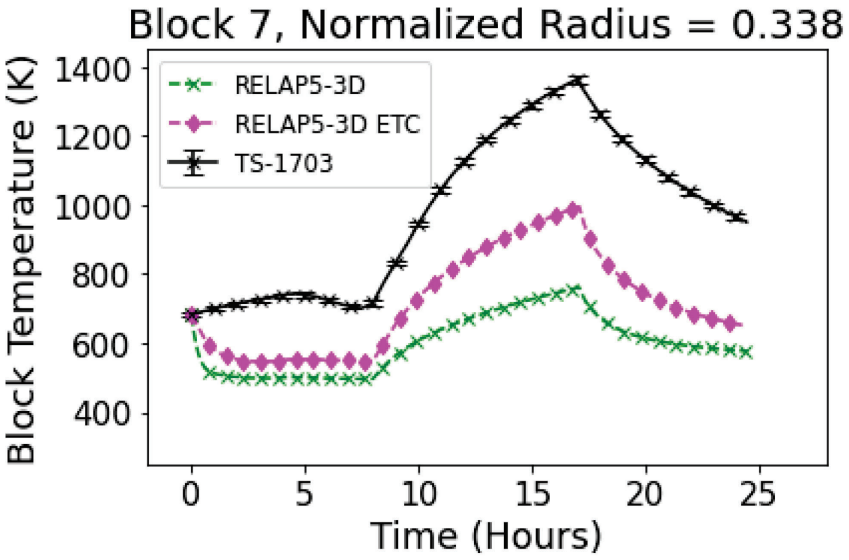

Figure 64. Temperature comparison for Ring 3 Block 7 in the primary sector.

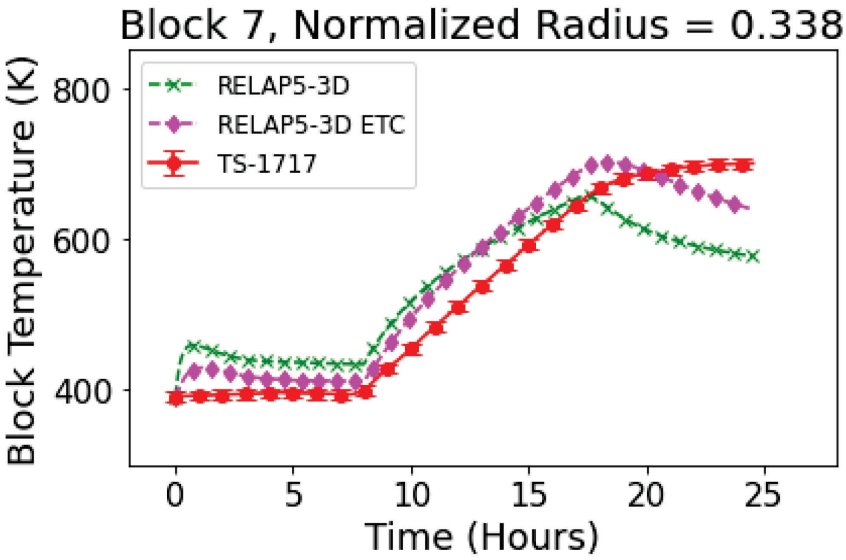

Figure 65. Temperature comparison for Ring 3 Block 7 in the secondary sector.

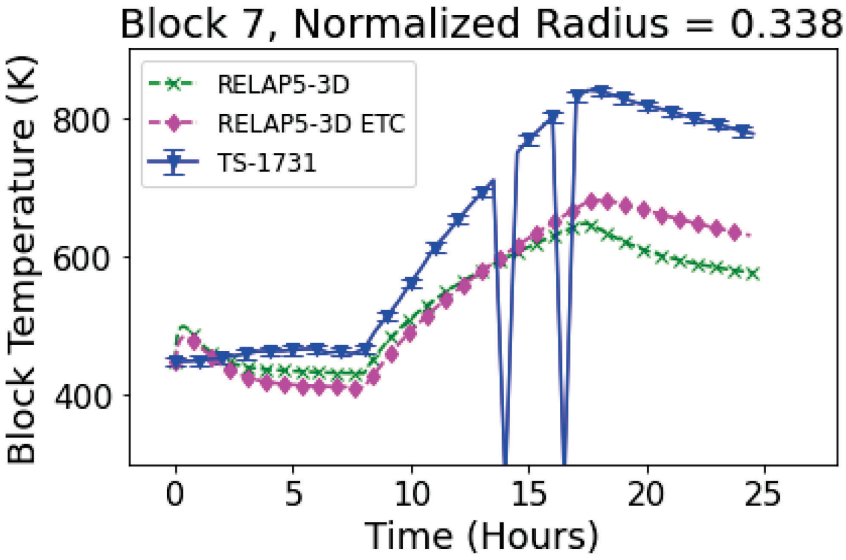

Figure 66. Temperature comparison for Ring 3 Block 7 in the tertiary sector.

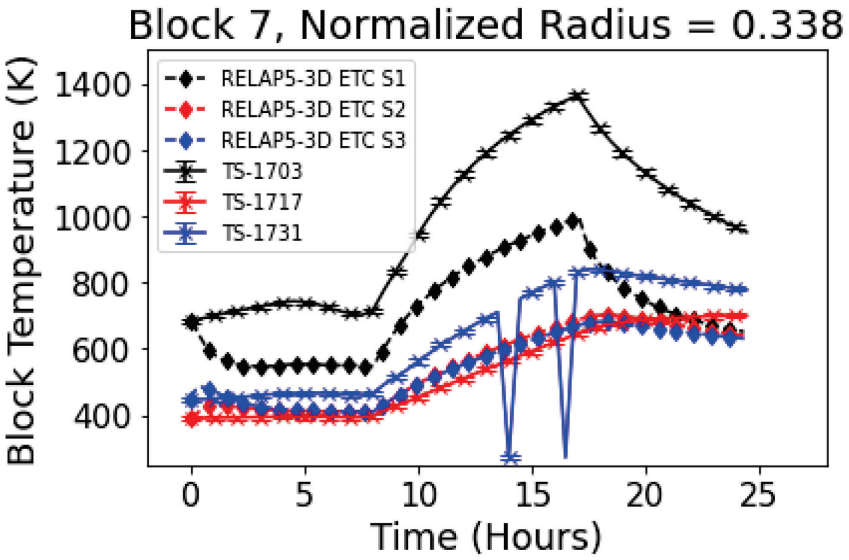

Figure 67. ETC temperature comparison for Ring 3 Block 7 for all sectors.

The next comparison focuses on the inner reflector (inner cylinder), corresponding to Position 1 in the test acceptance report. Figure 68 depicts the temperature data with the ETC model prediction. As can be seen, the temperatures in the RELAP5-3D model diverge from the experimental data at the beginning of the simulation and before the onset of the DCC. After the DCC begins, the model fails to capture the temperature trend and significantly underpredicts the magnitude of the temperature. Thus, the model was found to have insufficient agreement for the prediction of the inner cylinder temperatures.

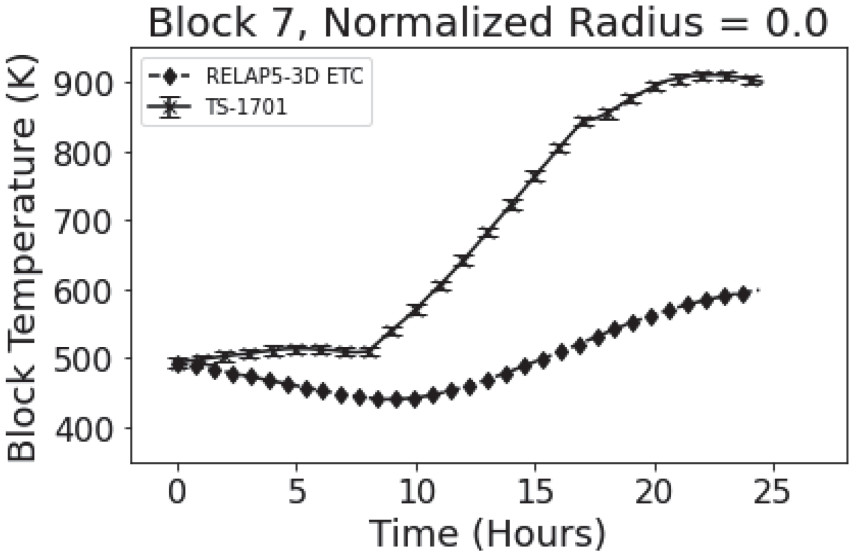

Figure 68. Temperature of the inner cylinder.

The helium temperature of Block 7 Ring 3 can be seen in Figure 69. The temperature comparisons between the new ETC model and the sensor data are similar to what is seen in Figure 67 with the heat structure block temperatures. The temperature trend is well predicted in all three sectors, but there are significant underpredictions in the peak temperature rises in the primary and tertiary sectors. Therefore,

the prediction of the primary and tertiary sectors has insufficient agreement with the experimental data, while the secondary sector has reasonable agreement.

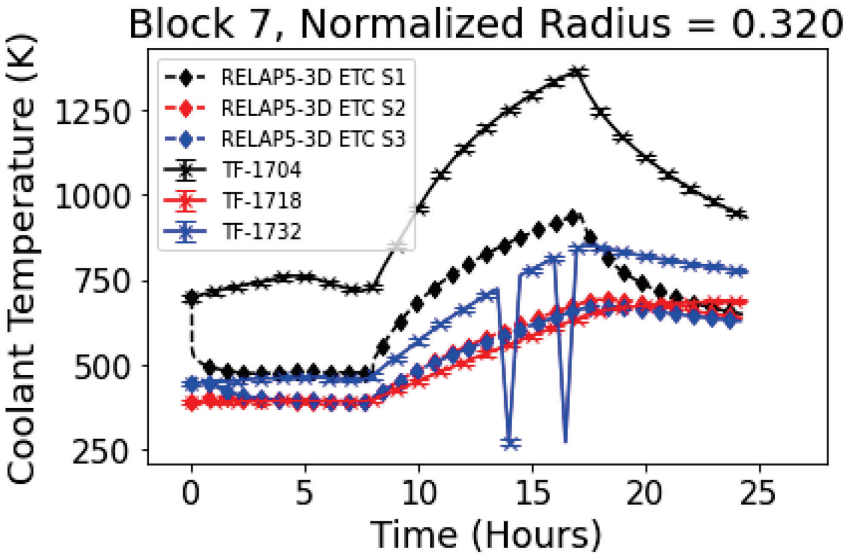

Figure 69. Helium temperature comparisons in Ring 3 Block 7 for all sectors.

Next, the block temperatures for Ring 8 of the heat structures can be seen in Figure 70. These temperatures are compared for the primary sector and the tertiary sector. The secondary sector sensor was omitted in the test acceptance report, so there is no comparison for this sector. One of the key findings within the experimental data is that the tertiary sector is considerably higher than the primary sector, which is an unexpected result. We expected the primary sector to have higher temperatures since there are more active heater rods than the tertiary sector, so it is unclear why it is significantly lower than the tertiary sector. On the other hand, the RELAP5-3D model predicts that the primary sector has a higher temperature rise than the tertiary sector. This could be indicative of the uniform heater power distribution assumption being incorrect. Further investigation will be needed in the future to determine why this discrepancy is occurring. Therefore, based on the experimental data, the RELAP5-3D prediction is determined to have insufficient agreement.

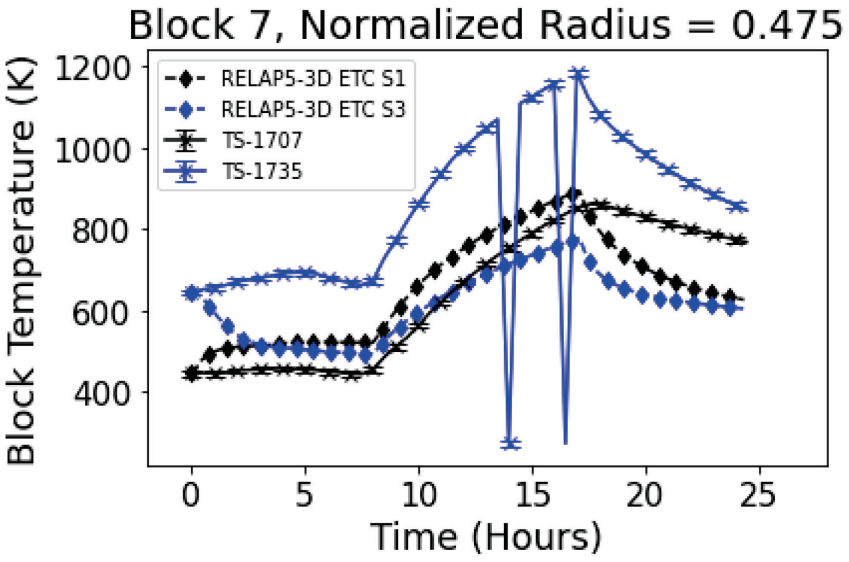

Figure 70. Temperatures for Ring 8 Block 7 for primary and tertiary sectors.

Figure 71 depicts the temperature comparison in the PSR for all three sectors. As can be seen, the behavior seen in the outer rings is also seen in the PSR. The temperature data indicates that the temperature in the tertiary sector is higher than the primary sector, further suggesting that the azimuthal power distribution is incorrect in the RELAP5-3D model. Therefore, the model is determined to have insufficient agreement in this prediction.

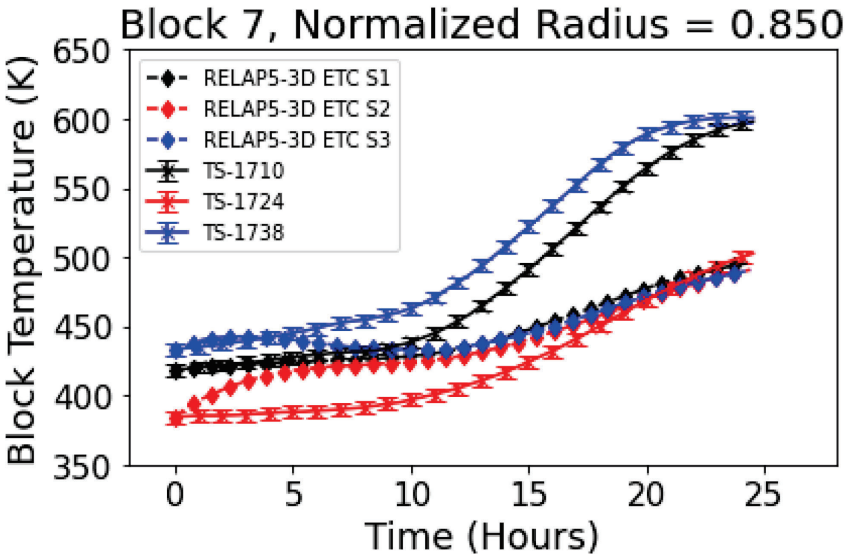

Figure 71. Temperatures for the PSR in Block 7 for all sectors.

Finally, Figure 72 illustrates the comparison of the RCCS coolant outlet temperature. The model and the experimental data appear to be in excellent agreement, with both models converging to a temperature of about 310 K.

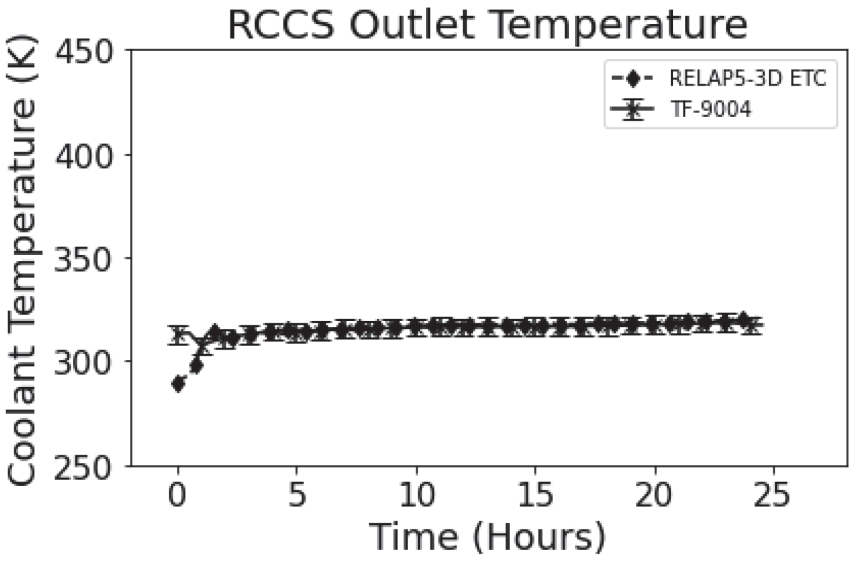

Figure 72. RCCS coolant outlet temperature.

5. CONCLUSIONS

In this report, we have presented results from Ex1 and Ex2 of the HTTF benchmark. For P2, we compare results between models in Ex1A and Ex1B. In that comparison, we saw generally similar behavior between the two models, but the new model showed a more detailed temperature profile radially. This is the expected result with the finer radial nodalization. The new model also experienced a slower long-term cooldown. The slower long-term cooldown was an unexpected result but likely stems from the change in radial heat transfer between the two models. In P2Ex1C, we saw similar trends to what was shown in P2Ex1B. Temperatures in the core change more rapidly in the new model during initial heatup and cooldown, but temperatures in the reflector rise slower and to lower peak values. In P3, we compared all exercises between models. For P3Ex1A and P3Ex1B, we saw the same and similar results to P2Ex1A and P2Ex1B, respectively. The results from P2Ex1B and P3Ex1B should be similar, because the higher pressure in the PCC is not sufficiently high to lead to a large impact from natural circulation. There is enough natural circulation to speed up the cooldown in both models relative to P2Ex1B, but the general behavior of the two transients is still quite similar. P3Ex1C represents a low-power steady state similar to PG-27. The very local heat generation provided an opportunity to highlight the difference in radial nodalization between the two models. Block temperatures were generally lower in most of the facility during P3Ex1C with the new model, but in the regions where heat was generated, the temperatures were generally higher in the new model. This result is consistent with expectations when the new model was developed. During P3Ex1D, the trends in temperature in the core were generally the same. The core reached higher temperatures in the new model than the legacy one, but reflectors heated up more slowly in the new model. Once again, the long-term heat removal was slower in the new model than in the legacy one. This result was unexpected and may suggest that the power density hypothesis was incorrect, or it may suggest that heat is removed from the core region more quickly in the new model, then gets removed more slowly from reflectors. Code-to-code comparisons revealed that temperature distributions behaved as expected in steady state, but transient temperature behavior differed from expectations.

In the validation studies for PG-27, we noticed substantial changes in the new model compared to the legacy model. In this study, we looked at the extended steady state before the onset of the PCC, which was also an opportunity to observe calibrations with the ETC in the new model. In the radial temperature distributions, we found that the calibrated ETC model demonstrated excellent agreement with the steady-state experimental data throughout the inner reflector and core regions. The ETC model began to

underpredict the temperature in the outer reflector and PSR regions. During the transient, the calibrated new model demonstrated substantial improvements in the temperature predictions in the active core region compared to the noncalibrated and legacy models. The ETC model began to underperform compared to the noncalibrated model in regions outside of the core. This indicated that the thermal conductivity and conductance used for the inner and outer reflectors may need to be investigated further. In addition, the RCCS coolant outlet temperature was also compared to the sensor data, and there was a significant overprediction in the outlet temperature in both versions of the new RELAP5-3D model, potentially indicating that too much heat is being transferred to the RCCS. When PG-27 results were compared between the legacy and new models, the new model was found to lead to significantly better prediction of local temperature in steady state, but the transient temperature behavior was comparable or worse. In the core regions, transient temperature rise during PG-27 was comparable between the legacy and new models, suggesting that perhaps the power density changes are less impactful on the transient than we expected. The improved transient temperatures in the core region are mostly a function of improved initial conditions. The predictions of temperature in the inner reflector are worse in the new model than in the legacy one, suggesting that there is significant need to revisit radial conduction in the new model. The improvements seen in the core regions is a positive step forward, but further work is needed for the inner and outer reflector, the PSR, and the RCCS.

Similar observations were seen for PG-29. The ETC calibration from PG-27 was also adopted for PG-29. The ETC model performed better in PG-29 than the nominal thermal conductivity model, particularly in sector 1 of the core. There are still underpredictions observed in the primary and tertiary sectors, but the agreement is improved over the noncalibrated new model. The legacy model cannot be accurately compared to temperatures from any sector, because it lacks any azimuthal discretization. The secondary sector appears to be well predicted, but it is important to keep in mind that error cancellation could be occurring, and further work needs to be done in the future. In the outer core region, the model greatly underpredicts the temperature in the tertiary sector, which had a notably higher temperature than the primary sector in the experimental data. The new model results predicted that the primary sector had a higher temperature than the tertiary sector. This unexpected discrepancy may indicate that our azimuthal power distribution assumptions may be incorrect, prompting the need for further investigation in these assumptions. Like PG-27, the new model underpredicts the temperatures in the inner reflector and PSR, indicating the need for further work in investigating the thermal conductivity and conductance assumptions in these regions.

Overall, we see that the new RELAP5-3D model provides similar temperature trends to the legacy model but an ability to capture greater detail. Code-to-code comparisons between the new and legacy models showed that the long-term transient heat removal in the new model was slower than in the legacy model due to changes in radial heat conduction, and a few block temperatures showed trends that require further investigation. Comparison to data from the steady-state portion of PG-27 showed reasonable to excellent agreement with block temperature distribution. This result alone shows an improvement over the legacy model. Transient predictions for PG-27 showed minimal to reasonable agreement. While this is the same level of agreement as the legacy model, the temperature predictions in the core region using the ETC showed improved predictions relative to those of the legacy model, but this is largely due to a shift in initial conditions and not due to better temperature rise predictions. The minimal agreement is introduced because of poor predictions of temperatures in the reflector regions. These predictions are the current state of work, but ongoing activities are modelling the reflectors using the nominal material thermal conductivity. This should provide a better set of results, because the reflectors contain few block penetrations to degrade their thermal conductivity. The PG-29 predictions show insufficient to minimal agreement, but the new model demonstrates predictions of temperatures for individual sectors—an improvement over the azimuthally symmetric legacy model. The work this year developing the new model has demonstrated valuable improvements and new capabilities for HTTF modeling, but further effort is required to validate the code against HTTF data.

5.1 Proposed Future Work

The work presented in this report is the current state of RELAP5-3D validation using the new HTTF model, but ongoing activities aim to further improve that model and to gain insight into a few eccentricities within the new and legacy models. Ongoing and future work includes the following activities:

- Investigate vessel temperature oscillation with node length (Both models)
- Investigate block 9 temperatures in P3x1C (New model)
- Investigate RCCS temperatures in P2Ex2 models (New model)
- Re-run P3Ex2 with nominal thermal conductivity in the reflectors
- Investigate radial conduction models to ensure the higher thermal resistances in the new model are not too high

These planned activities will provide us with further insight into the performance of the new model and may improve the agreement between model and experiment.

6. REFERENCES

1. Strydom, G., A. S. Epiney, A. Alfonsi, and C. Rabiti. 2017. "Comparison of the PHISICS/RELAP5-3D ring and block model results for phase I of the OECD/NEA MHTGR-350 benchmark." *Nuclear Technology*, 193(1): 15–35. http://dx.doi.org/10.13182/NT14-146.
2. Lu, C. and N. R. Brown. 2019. "Fully ceramic microencapsulated fuel in prismatic high-temperature gas-cooled reactors: Design basis accidents and fuel cycle cost." *Nuclear Engineering and Design*, 347: 108–121. https://doi.org/10.1016/j.nucengdes.2019.03.022.
3. Gorton, J. P. and N. R. Brown. 2020. "Defining the performance envelope of reactivity-initiated accidents in a high-temperature gas-cooled reactor." *Nuclear Engineering and Design*, 370. https://doi.org/10.1016/j.nucengdes.2020.110865.
4. Ghezzi, C. G., R. F. Kile, and N. R. Brown. 2022. "TRISO SiC Failure Probability for Reactivity Initiated Accidents in High-Temperature Gas-Cooled Reactors." *Nuclear Science and Engineering*, 196(11): 1361–1382. https://doi.org/10.1080/00295639.2022.2097466.
5. Duchnowski, E. M., R. F. Kile, K. Bott, L. L. Snead, J. R. Trelewicz, and N. R. Brown, "Pre-conceptual high temperature gas-cooled microreactor design utilizing two-phase composite moderators. Part I: Microreactor design and reactor performance." *Progress in Nuclear Energy*, 149:104257. https://doi.org/10.1016/j.pnucene.2022.104257.
6. Shiozawa, S., S. Fujikawa, T. Iyoku, K. Kunitomi, and Y. Tachibana. 2004. "Overview of HTTR design features." *Nuclear Engineering and Design*, 233(1–3): 11–21. https://doi.org/10.1016/j.nucengdes.2004.07.016.
7. Woods, B. 2019. "OSU High Temperature Test Facility Design Technical Report, Revision 2." OSU-HTTF-TECH-003-R2, Oregon State University, Corvallis, OR. https://www.osti.gov/biblio/1599410.
8. Epiney, A. S. et al. 2022. "Overview of HTTF Modeling and Benchmark Efforts for Code Validation for Gas-Cooled Reactor Applications." In proceedings *Fourth International Conference on Generation IV & Small Reactors (G4SR-4)*, Toronto, ON, Canada.

9. Bayless, P. D. 2018. “RELAP5-3D Input Model for the High Temperature Test Facility.” INL/EXT-18-45579, Idaho National Laboratory, Idaho Falls, ID. https://inldigitallibrary.inl.gov/sites/sti/sti/Sort_5548.pdf.
10. Kile, R. F., A. S. Epiney, and N. R. Brown. 2023. “RELAP5-3D Solutions to Exercise 1 of the OECD-NEA HTTF Benchmark.” In proceedings *Transactions of the American Nuclear Society*, Indianapolis, IN. https://www.ans.org/pubs/transactions/article-53491/.
11. Kile, R. F., A. S. Epiney, and N. R. Brown. 2023. “High Temperature Test Facility sensitivity and calibration studies to inform OECD-NEA benchmark calculations.” *Nuclear Engineering and Design*, 404:112178. https://doi.org/10.1016/j.nucengdes.2023.112178.
12. Epiney, A. S. 2020. “RELAP5-3D Modeling of High Temperature Test Facility Test PG-26.” INL/EXT-20-29902, Idaho National Laboratory, Idaho Falls, ID. https://inldigitallibrary.inl.gov/sites/sti/sti/Sort_26774.pdf.
13. Gairola, A. and A. S. Epiney. 2021. “RELAP5-3D Simulations of PG-27INL/EXT-21-63798, Idaho National Laboratory, Idaho Falls, ID.
14. Kile, R. F., A. S. Epiney, and N. R. Brown. 2024. “RELAP5-3D validation studies based on the High Temperature Test facility.” *Nuclear Engineering and Design*, 426:113401. https://doi.org/10.1016/j.nucengdes.2024.113401.
15. Woods, B. 2019. “Instrumentation Plan for the OSU High Temperature Test Facility, Revision 4.” OSU-HTTF-TECH-002-R4, Oregon State University, Corvallis, OR.
16. Schultz, R. R. 1993. “International Code Assessment and Applications Program Summary of Code Assessment Studies Concerning RELAP5/MOD3, and TRAC-B.” NUREG/IA-0128, U. S. Nuclear Regulatory Commission, Rockville, MD. https://www.nrc.gov/reading-rm/doc-collections/nuregs/agreement/ia0128/index.html.
17. Halsted, J. and I. Gutowska. 2023. “Verification and validation of a lower plenum mixing test at the OSU High Temperature Test Facility.” *Nuclear Engineering and Design*, 406:112251. https://doi.org/10.1016/j.nucengdes.2023.112251.
18. Kile, R. F. and A. S. Epiney. 2024. “Development of an Improved RELAP5-3D Model for the High Temperature Test Facility.” In proceedings *Advances in Thermal Hydraulics*, Orlando, FL.
19. Hua, T., R. Kile, S. N. Lee, L. Zou, and A. Epiney. 2024. “Code Benchmark of Pressurized Conduction Cooldown Transient in the High Temperature Test Facility.” In proceedings *International Congress on Advances in Nuclear Power Plants*, Las Vegas, NV. https://www.ans.org/pubs/proceedings/article-56378/.